ISSN: 2331-1959 Volume 9, Number 2, April 2021

Scientific Research Publishing

Archaeological Discovery

ISSN: 2331-1959

https://www.scirp.org/journal/ad

Journal Editorial Board

ISSN Print: 2331-1959 ISSN Online: 2331-1967

https://www.scirp.org/journal/ad

Archaeological Discovery, 2021, 9, 85-150
https://www.scirp.org/journal/ad
ISSN Online: 2331-1967
ISSN Print: 2331-1959

Table of Contents

Volume 9 Number 2 April 2021

Archaeological Discovery (AD)
Journal Information

SUBSCRIPTIONS

The *Archaeological Discovery* (Online at Scientific Research Publishing, https://www.scirp.org/) is published quarterly by Scientific Research Publishing, Inc., USA.

Subscription rates:
Print: $39 per issue.
To subscribe, please contact Journals Subscriptions Department, E-mail: sub@scirp.org

SERVICES

Advertisements
Advertisement Sales Department, E-mail: service@scirp.org

Reprints (minimum quantity 100 copies)
Reprints Co-ordinator, Scientific Research Publishing, Inc., USA.
E-mail: sub@scirp.org

COPYRIGHT

PRODUCTION INFORMATION

For manuscripts that have been accepted for publication, please contact:
E-mail: ad@scirp.org

Archaeological Discovery, 2021, 9, 85-90
https://www.scirp.org/journal/ad
ISSN Online: 2331-1967
ISSN Print: 2331-1959

Radiodating of the Hairs of the Presumed Holy Maria-Magdalena

Gérard Lucotte

Institut d'Anthropologie Moléculaire, Paris, France
Email: lucotte@hotmail.com

How to cite this paper: Lucotte, G. (2021). Radiodating of the Hairs of the Presumed Holy Maria-Magdalena. *Archaeological Discovery, 9,* 85-90.
https://doi.org/10.4236/ad.2021.92004

Received: January 13, 2021
Accepted: March 6, 2021
Published: March 9, 2021

Abstract

We report here the result concerning the radiodating of the carbon of the keratin of hairs from a lock of the presumed Holy Maria-Magdalena kept in the Saint-Maximin basilica. The aim of this research is to establish the best dating possible. The age obtained is 1260 ± 30 years; for this hair lock this date corresponds in fact to that of the exhumation of Maria-Magdalena's body by Charles II in 1279. We conclude that King Charles II had completely carried out this exhumation story, to reinforce the influence of some part of his territory at that time.

Keywords

Maria-Magdalena's Hairs, Radiodating, Carbon of the Keratin, 1279 Exhumation, Charles II

1. Introduction

Holy Maria-Magdalena (3?-63?) is the most abundantly cited women in the four Gospels. According to the French "tradition des Saints de Provence" (Trouillet, 2016) she-and her companions landed on the present French Mediterranean shores (in a region corresponding to the current part of Les-Saintes-Maries-de-la-Mer) and reached the towns of Marseilles and Aix-en-Provence. Details about the exhumation of the Maria-Magdalena's remains which are at the basis of this tradition are given by King Charles II (1248-1309), who exhumed these remains in 1279 (at this time he was only titled Prince of Salerne) near the "prieuré" (clergy house) of the village of Saint-Maximin.

Some relics of the presumed Maria-Magdalena were kept in the Saint-Maximin basilica, where a large lock of Maria-Magdalena's hair is conserved in a dedicated reliquary. I have obtained some hairs of this lock, for scientific purpose

(microscopic examinations and chemical analyses). We have published these last year three initial papers: on the mitochondrial DNA haplogroup found by extracting genomic DNA from the bulb of hair number 10 (Lucotte, 2016), on the explanation of the observed brown-red colour of the hairs by scanning electron microscopic characterization of its melanosomes (Lucotte & Thomasset, 2017), and on the description of some fennel rests on or at the vicinity of some of these hairs (Lucotte et al., 2018).

Remarkable results were obtained concerning a new protocol for radiocarbon dating of the keratin of hairs (Richardin et al., 2011). The research purpose of the present study is to use this sort of protocol for the radiocarbon dating of the keratin of three hairs of the presumed Maria-Magdalena.

2. Material and Methods

Figure 1 shows the three hairs used for the radiodating; they are the eleventh to thirteenth hairs of the kept lock.

These hairs of the lock were not studied for other thing that radiodating (they were only examined previously by optic microscopy), contrary to the ten first (Lucotte, 2016) that were analysed for electron microscopy and chemistry.

Radiodating of the ^{14}C of these hairs was carried out by the Company Beta-Analytic Inc. (Miami, USA). It is an original method of radiodating, consisting in the measurement of the carbon radioisotope of the keratin of the hairs.

3. Results

Figure 2 summarizes the results obtained for the radiocarbon dating; the calibration curve is intercepted by radiocarbon ages at the values of 1 or 2 sigmas. The 2 sigmas (95% of probability) calibrated (Cal) results for the three values of the curve area: Cal AD (after J.-C.) 670 to 780, Cal BP (in radiocarbon years) 1280 to 1170; Cal AD 790 to 810, Cal BP 1160 to 1140; Cal AD850, Cal BP1100.

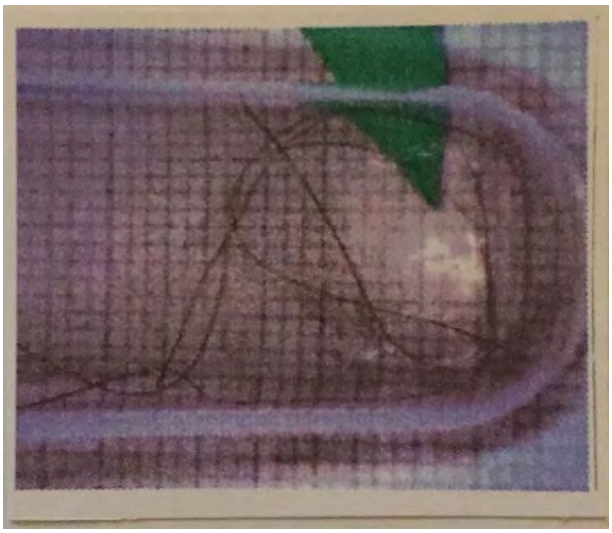

Figure 1. Photograph of three hairs used for the radiodating.

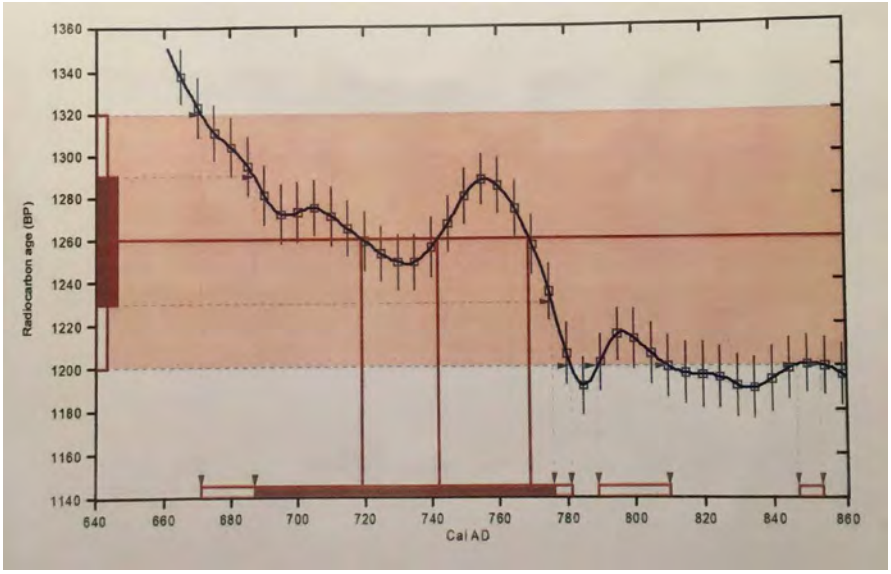

Figure 2. Calibration of radiocarbon age to calendar years.

Intercepts radiocarbon age with the calibration curve area: Cal AD720 (Cal BP1230); Cal AD740 (Cal BP1210); Cal AD 770 (Cal BP1180).

The 1 sigma (68% of probability) calibrated results is: Cal AD 690 to 780 (Cal BP 1260 to 1170).

The final result for age is: 1260 ± 30 years. Remarkably these values correspond to 1279, that is the date of exhumation of Maria-Magdalena's remains by Charles II.

4. Discussion

Results reported here on an original method of radiodating of the carbon of the keratin of the hairs establish that they are certainly not those of Holy Maria-Magdalena, who lived ≈ 3 - 63. These hairs are kept in the Saint-Maximin basilica, and are known as those of the presumed Maria-Magdalena. Moreover, the date obtained (1260 ± 30 years) corresponds to that (1279) of the exhumation of the presumed Maria-Magdalena by Charles II. He at that time-King (1248-1303) had indeed exhumed the body of the presumed Holy Maria-Magdalena in 1279, near the clergy House of the Saint-Maximin village.

The priest Etienne-Michel Faillon (1789-1870), a native of the Tarascon village, published in 1848 (Faillon, 1865) a monumental work of two volumes, totalling about 1500 pages with the goal to demonstrate by historical proof that Maria-Magdalena and her companions have truly lived in Provence at the first Century. But all the Failllon's arguments were systematically refuted in the middle of the XXth Century by Mgr Victor Saxer (Saxer, 1959); he claimed "Being the silence observed before 1279 at Saint-Maximin concerning Holy Maria-Magdalena, we are well founded to say that she was not honoured in that site of Provence since the late period of the XIIIth Century".

As implication research of our own contribution to the question, we now ex-

amined the "authentication proofs" concerning Maria-Magdalena's hairs we established in our previous publications.

In our second 2019 publication (Lucotte, 2019) we showed that deposits of calcium phosphate were observed on most of the hairs studied. We know that hairs covered the cranium in the historical (between 1283 and 1793) bust-reliquary where Maria-Magdalena's remains were kept; it is during this long period of time that the hydroxyapatite of the osseous cranium transferred to the hairs.

In the same publication we showed that there are some particles of gold (of a gold powder, some of them being of pure gold and other of an alloy of gold, silver and copper) on several of the hairs studied. Probably most of them (particularly those that are of pure gold) are due to close contact between hairs and the gold of the bust-reliquary (of gold) or/and of the crown of Charles I (Charles II's father) that was transferred to the hairs. Similarly particles of silver sulphide and chloride, of silver and gold and of silver and copper that we observed on the surface of some hairs studied were explained by the fact that these hairs (and other remains) were initially since 1281-kept in a silver reliquary.

In our 2018 publication (Lucotte et al., 2018) we established that fennel (*Foeniculum vulgare*) residues—pollen grains, foliar, pedicular and stem debris are found on, or at the proximity of some of the hairs studied. That confirms some details concerning the Maria-Magdalena discovery on 19 of December 1279, reported by Bernard Gui (Faillon, 1865) forty years after the facts.

But all these observations (about calcium phosphate, gold, silver and fennel) concern the remains exhumed in 1279, not Holy Maria-Magdalena *per se*.

In our second 2020 publication (Lucotte, 2020), we observed six marble particles on the surfaces of the hairs studied. These marble fragments are similar to those of the sarcophagis "de Marie-Madeleine" and "de Saint Sidoine" that one can see today in the crypt of the Saint-Maximin basilica. Our interpretation is that these marble fragments deposited on the surface of the hairs could originate from the walls of the sarcophagis and especially from the second one where we knew (Faillon, 1865) that Maria-Magdalena was buried before the 1279 exhumation. Our findings have some relative importance because previously (Fixot, 2009) there were in fact no formal proofs that Maria-Magdalena's body was buried initially in one or another of these sarcophagis.

Remains of the skeleton exhumed in 1279 mainly the cranium and the mandible, from Saint-Maximin; a fragment of tibia and some hairs, from La-Sainte-Baume; a piece of femur, from the Madeleine's church of Paris, were studied in a physical anthropology perspective (Saxer, 1977). The conclusions of this study agree more with that of an individual of the Mediterranean type, probably a woman, aged of about 50 years old.

What are the characteristics of the hairs from the body exhumed in 1279?

They are from a woman of maternal Jewish ancestry. This was established (Lucotte, 2016) by the amelogenin test and by mitochondrial DNA characteriza-

tion on the genomic DNA extracted from the bulb of the hair number 10. Such a maternal Jewish ancestry was already worded in the Golden Legend (de Voragine, 2004), that was the main religious book which was largely diffused through Europe in the second half of the XIIIth Century.

They are of red-brown colour. This red coloration is not due to some sort of dyeing, but is the natural colour of the hair melanosomes (Lucotte & Thomasset, 2017). The story of the corresponding lock of hair is somehow tortuous, but ever these hairs (located in transparent containers) were available to observers. That explains why the most famous representations of Maria-Magdalena concern paintings showing her with red-brown hairs (mainly from the XVth Century)

They are covered by marine remains (Lucotte et al., 2019). These remains: some mineral particles and micro-organisms (of vegetal and animal natures) adhering to the hairs, indicate a close past—contact of these hairs with the sea water. Such a finding is incompatible with that of Maria-Magdalena in the last period of her life, retired for thirty years in a cave of the mountains of the Sainte-Baume (Faillon, 1865).

These hairs were also covered by skin debris (Lucotte et al., 2020b): skin-cells, dandruffs, and other skin materials of various sorts like skin shreds. One of them (the hair number 9) is covered by a piece of scalp; it corresponds to the customary conservative procedure (with salt), that was probably used for the preservation of the precious skin tissue named the *Noli me tangere* (Faillon, 1865).

These hairs were also intensely infected by nits of louse (Lucotte et al., 2020a), a common complaint of adults in the past times.

5. Conclusion

The radiodating of the keratin carbon of the hairs kept in the Saint-Maximin basilica, which are from the presumed Holy Maria-Magdalena, has given in fact a date of 1260 ± 30 years. This date frames that of 1279, which was the exhumation of Maria-Magdalena by Charles II, King of Napoli and Count of Provence, Anjou and Maine. The significance of the present study is that it is highly probable that Charles II had completely fabricated this exhumation story, to reinforce the influence of one urban centre of his territory.

Acknowledgements

I thank F. Racine, the priest of the Saint-Maximin-la-Sainte-Baume basilica, who furnished Maria-Magdalena's hairs. Thank you also to Dr C. Patrick, Deputy Director of Beta Analytic, who provided precise information about this radiodating. I thank also the French association UNEC (W. Wuermeling) for financial support of this work.

Conflicts of Interest

The author declares no conflicts of interest regarding the publication of this paper.

References

de Voragine, J. (2004). *La légende dorée*. Paris: Gallimard Ed.

Faillon, E. M. (1865). *Monuments inédits sur l'apostolat de sainte Marie Madeleine en Provence, et sur les autres apôtres de cette contrée, saint Lazare, saint Maximin, sainte Marthe, les saintes Marie Salomé et Jacobé*. Paris: Migne Ed.

Fixot, M. (2009). *La crypte de Saint-Maximin-La-Sainte-Baume*. Saint-Rémy-de-Provence: Edisud Ed.

Lucotte, G. (2016). The Mitochondrial DNA Mitotype of Sainte Marie-Madeleine. *International Journal of Sciences, 5,* 10-19. https://doi.org/10.18483/ijSci.1167

Lucotte, G. (2019). Silver and Gold on the Hairs of Holy Maria-Magdalena, Studied by Scanning Electron Microscopy and Elemental Analysis. *Archaeological Discovery, 7,* 257-282. https://doi.org/10.4236/ad.2019.74012

Lucotte, G. (2020). Mineral Particles Found on the Hairs of Holy Maria-Magdalena Studied by Scanning Electron Microscopy and Elemental Analysis. *Open Journal of Applied Sciences, 10,* 41-59. https://doi.org/10.4236/ojapps.2020.103004

Lucotte, G., & Thomasset, T. (2017). Study of the Red Colour of Ste Marie-Madeleine (≈3-63) Hair by Scanning Electron Microscopic Characterization of Its Melanosomes. *Journal of Dermatology and Pigmentation Research, 1,* 1-9.

Lucotte, G., D'Hérissart, E., & Thomasset, T. (2019). Marine Micro-Remains on Holy Maria-Magdalena's Hair, Studied by Scanning Electron Microscopy and Elemental Analysis. *Archaeological Discovery, 7,* 155-191. https://doi.org/10.4236/ad.2019.73009

Lucotte, G., Izri, A., & Thomasset, T. (2020a). Nits of Louse on the Hairs of Holy Maria-Magdalena: A SEM-EDX Study. *Global Dermatology, 7,* 1-4.

Lucotte, G., Thomasset, T., & Borensztajn, S. (2020b). Slin Debris on the Hairs of Holy Maria-Magdalean: A SEM-EDX Analysis. *International Journal of Sciences, 9,* 57-79. https://doi.org/10.18483/ijSci.2273

Lucotte, G., Thomasset, T., & Salmon, A. (2018). Fennel (*Foeniculum vulgare*) Rests on the Holy Maria-Magdalena Hairs, Studied by Scanning Microscopy and Elemental Analysis. *Archaeological Discovery, 6,* 216-270. https://doi.org/10.4236/ad.2018.63012

Richardin, P., Gandolfo, N., Carminati, P., & Walter, P. (2011). A New Protocol for Radiocarbon Dating of Hair and Keratin Type Samples—Application to an Andean Mummy from the National Museum of Natural History in Paris. *Archaeological and Anthropological Sciences, 3,* 379-384. https://doi.org/10.1007/s12520-011-0070-3

Saxer, V. (1959). *Le culte de Marie-Madeleine en Occident, des origines à la fin du Moyen-Age*. Auxerre: Society of Archaeological Digs of Yonne Ed.

Saxer, V. (1977). Les ossements dits "de sainte Marie Madeleine" conservée à Saint-Maximin-la-Sainte-Baume. *Provence Historique, 27,* 257-311.

Trouillet, M. C. (2016). *Les Reliques de Ste Marie-Madeleine*. Aix-en-Provence: Petrus Ed.

Archaeological Discovery, 2021, 9, 91-112
https://www.scirp.org/journal/ad
ISSN Online: 2331-1967
ISSN Print: 2331-1959

A Reassessment on the Lithic Artefacts from the Earliest Human Occupations at Puente Rock Shelter, Ayacucho Valley, Peru

Juan Yataco Capcha[1], Hugo G. Nami[2], Wilmer Huiza[1]

[1]Archaeological and Anthropological of San Marcos University Museum, Lima, Perú
[2]Department of Geological Sciences, Laboratory of Geophysics "Daniel A. Valencio", CONICET-IGEBA, FCEN, UBA, Buenos Aires, Argentina
Email: jyatacoc_ac@unmsm.edu.pe

How to cite this paper: Capcha, J. Y., Nami, H. G., & Huiza, W. (2021). A Reassessment on the Lithic Artefacts from the Earliest Human Occupations at Puente Rock Shelter, Ayacucho Valley, Peru. *Archaeological Discovery, 9,* 91-112.
https://doi.org/10.4236/ad.2021.92005

Received: February 14, 2021
Accepted: March 22, 2021
Published: March 25, 2021

Abstract

Richard "Scotty" MacNeish, between 1969 and 1972, led an international team of archaeologists on the Ayacucho Archaeological-Botanical—Project in the south-central highlands of Peru. Among several important archaeological sites identified there, MacNeish and his team excavated the Puente rock shelter. As a part of an ongoing research program aimed to reassess the lithic remains from this endeavor, we re-studied a sample by making diverse kinds of morpho-technological analysis. The remains studied come from the lower strata at Puente, where a radiocarbon assay from layer XIIA yielded a calibrated date of 10,190 to 9555 years BP that the present study identifies, various activities were carried out at the site, mainly related to manufacturing and repairing unifacial and bifacial tools. The artifacts studied are comparable with the lithic remains found in other sites located in the Ayacucho Basin, and with other early evidence from other parts of the south-central Andes.

Keywords

Lithic Analysis, Late Pleistocene/Early Holocene Archaeology, South America, Peru, Ayacucho Basin

1. Introduction

Headed by Richard MacNeish (Robert S. Peabody Institute of Archaeology), between 1969 and 1972, an interdisciplinary team of archaeologists carried out the "Ayacucho Archaeological-Botanical Project" in the Ayacucho Basin, highland Peru (e.g., MacNeish, 1969, 1981; MacNeish et al., 1970, 1980). Becoming a

seminal research in the Americas' archaeological history (Dillehay, 1985), this project allowed the excavation of several sites. Worth mentioning are the Pikimachay, Ayamachay, and Rosamachay caves, as well as Jaywamachay and the Puente rock shelters. These sites, and particularly the latter, revealed a remarkable archaeological record spanning from the Late Pleistocene to historical times. Several volumes have provided very much data, information and results of this investigation. However, the reported lithic artefacts lack standard definitions, detailed studies, and associations with other sites; hence, this evidence should be better organized based on comprehensive reviews. In pursuing this goal, a detailed revision on the Ayacucho-Huanta Project collections is being carried out, as well as new fieldwork in the area. As a part of this ongoing research, this paper reports the lithic analysis of the specimens belonging from the lowest strata of the Puente site (**Figure 1**), and observations on a few remarkable bone remains.

Figure 1. Location of Puente site in Ayacucho Basin, Peru (from Google Earth Pro 2020).

2. Excavations, Stratigraphy and Chronology

The Puente rock-shelter (Ac158) was located in the Department of Ayacucho, northeast of the Huamanga (13˚8'7.70"S, 74˚12'49.17"W, 2640 m.a.s.l.). At the base of its talus is the usually dry Wichqana Creek. The site takes its name from *Puente Totorilla*, a nearby bridge. Its excavators suggested that the rock shelter slope was the eroded remnant of a terrace formed by the collapse and erosion of the cave's ceiling (MacNeish, 1969: p. 24; MacNeish, 1981: p. 82). The site has been destroyed by use of heavy machinery during agricultural activities (**Figure 2(a)** & **Figure 2(b)**).

In 1969, A. García Cook and MacNeish excavated a trench of 9 m long by 1 m wide, reaching two meters depth (MacNeish, 1981: pp. 83-84, fig. 4-2 to 4-7). A team directed by García Cook (**Figure 3**), in 1970, excavated a large surface using a one square meter grid (**Figure 4**). Several unpublished images depict the deposit's depth, as well as different views during the field-work (**Figures 5(a)-(d)**). The excavation showed that the site was inhabited by different human occupations thought time, mainly of pre-ceramic nature (MacNeish, 1969: pp. 17-24, 31-33; MacNeish et al., 1970: pp. 5-16, 31-34).

Figure 2. (a) General view of Puente site from the Wichqana creek; (b) Current condition due to machinery impact. Except when clearly expressed otherwise, all the pictures are by J. Yataco Capcha.

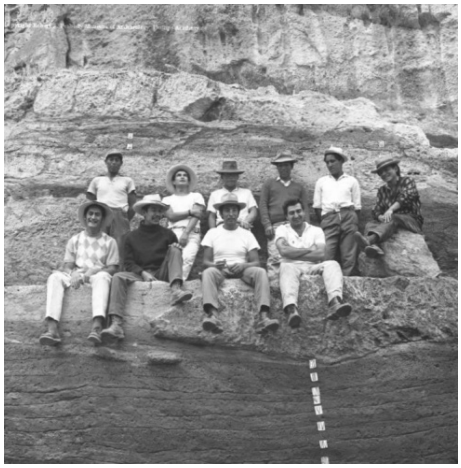

Figure 3. The Ayacucho Archaeological-Botanical Project team members during the excavations of the Puente site in 1970. Sitting from left to right: V. Cárdenas, A. García Cook, unknown, and E. Sáenz; standing: unidentified laborers (Copyright: Robert S. Peabody Institute of Archaeology, Phillips Academy).

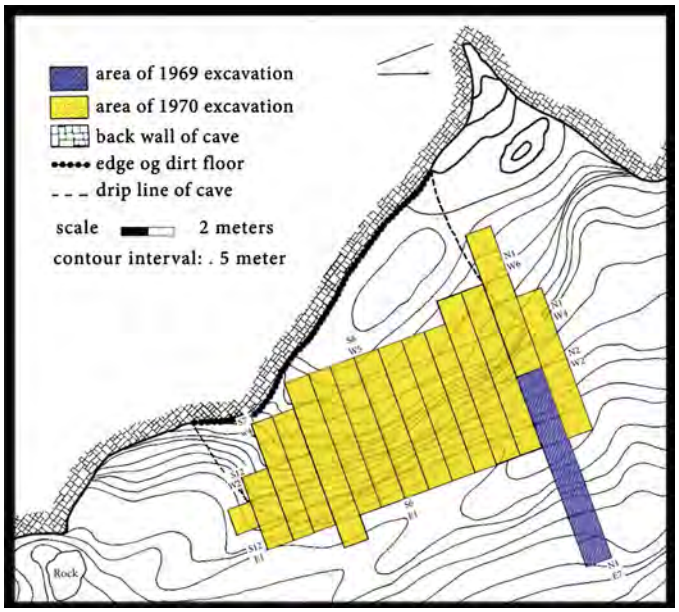

Figure 4. Puente site floor plan (modified after Cook and MacNeish, 1981: p. 81, fig. 4-1).

Figure 5. Images of the Puente rock-shelter excavations performed in 1969 (a) and 1970 (b)-(d). (a) Opening the initial trench; (b) Recording the stratigraphy in the step trenches; (c) M. Benavides working on north-south cross trench at the beginning of the season; (d) C. Chaud sieving sediments (Copyright: Robert S. Peabody Institute of Archaeology, Phillips Academy).

Stratigraphic analysis identified fourteen layers, called "zones" (*cf.* MacNeish, 1981: pp. 88-89, fig. 4-10; MacNeish et al., 1983: pp. 50-57). The deposit's depth varies according to its location on the site. This paper focuses on material from strata XIIA to XIV, located in the front part of the rock shelter's talus, and indicated with colors in **Figure 6**. A brief description is as follows: XIIA is ~8 cm thick formed by yellowish-brown sediment. Covering a surface of ~87 square meters, layer XIII is light brown sediment with yellowish spots ~15 cm thick. Finally, XIV is the deepest stratum deposited over the bedrock. It is composed of light yellow colored sediment mixed with volcanic ash. Concerning the archaeological finds, the most abundant remains come from layer XIIA-XIII, while XIV yielded the smallest quantity from grids S4, S5, S4E1, S6E1, and S7E1.

As depicted in **Figure 7**, ten radiocarbon assays on charcoal samples were obtained from the excavation (Ziólkowski et al., 1994). They were calibrated using the OxCal v4.3 program and the SHCal13 southern hemisphere calibration curve (Bronk Ramsey & Lee, 2013; Hogg et al., 2013). Additionally, the results agree with the stratigraphic provenance of the samples. Furthermore, the majority of the dates (n = 9) spanned the ~7 - 8 kya cal period. The earliest assay of 8860 ± 125 uncalibrated years BP (Ziólkowski et al., 1994: p. 330) coming from stratum XIIA is 10,190 to 9555 calibrated years BP (**Figure 8**). Considering the dates, layers XIIA-XIII belong to the early Holocene, and probably layer XIV, to the Pleistocene-Holocene transition/Holocene.

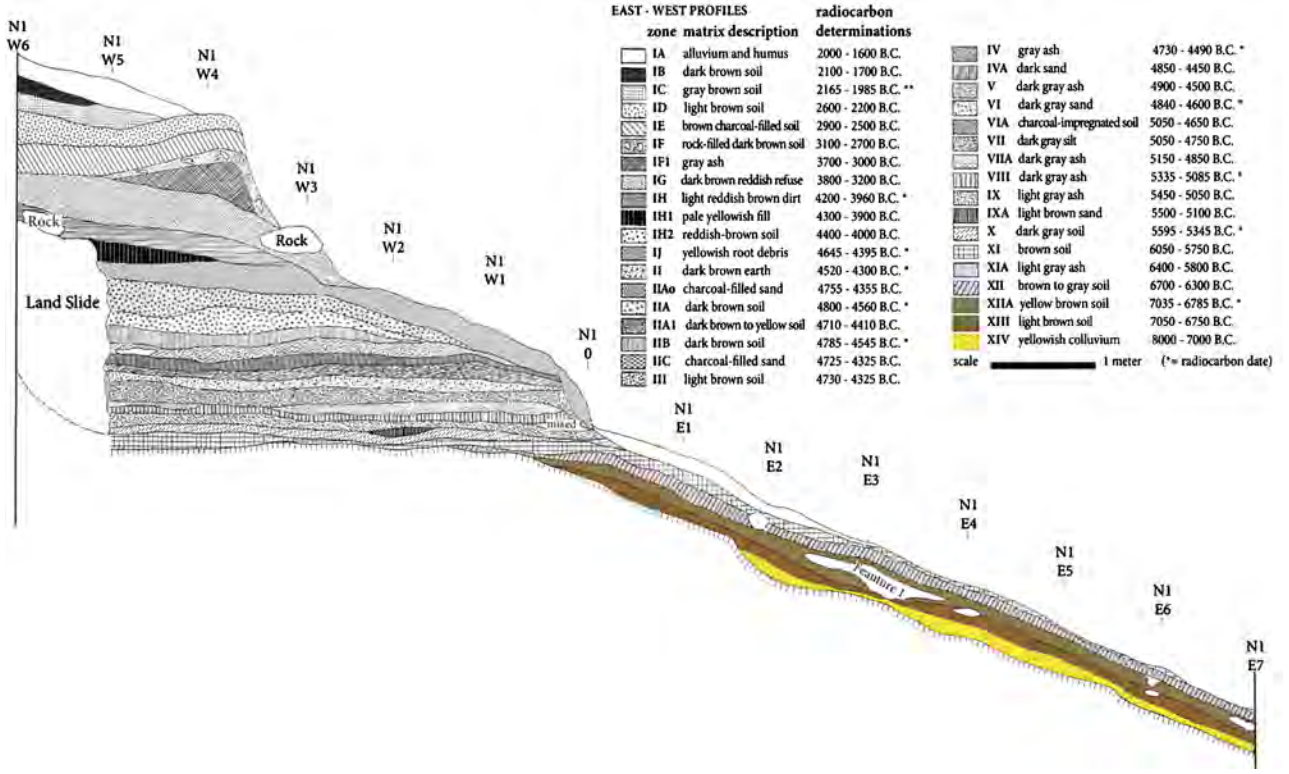

Figure 6. Detailed stratigraphic sequence recorded in the east–west section of the Puente rock shelter. Redrawn from García Cook et al. (1981: pp. 88-89, fig. 4-10).

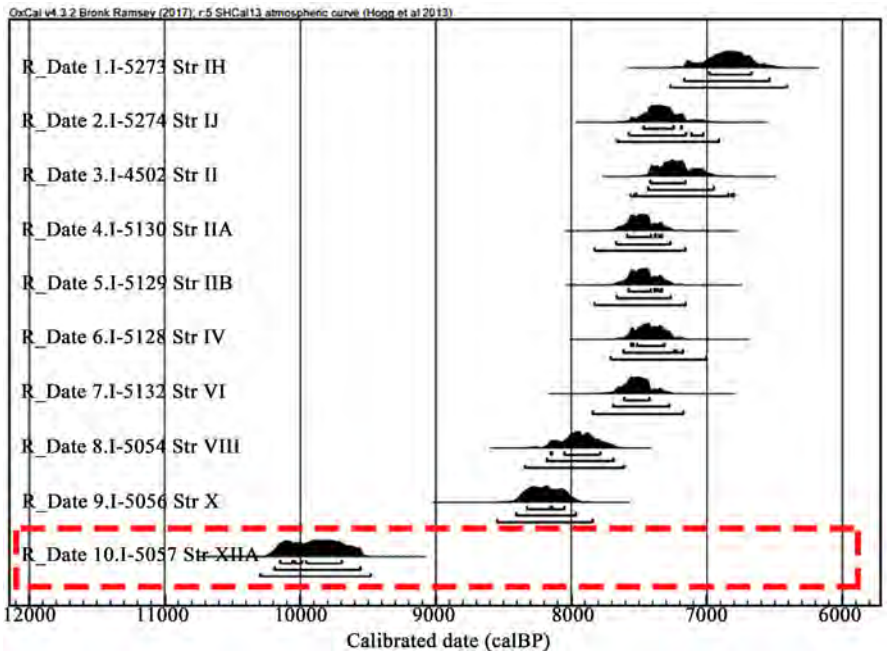

Figure 7. Calibrated radiocarbon ages of the Puente rock-shelter. The red rectangle with dashed lines indicates the earliest date at the site.

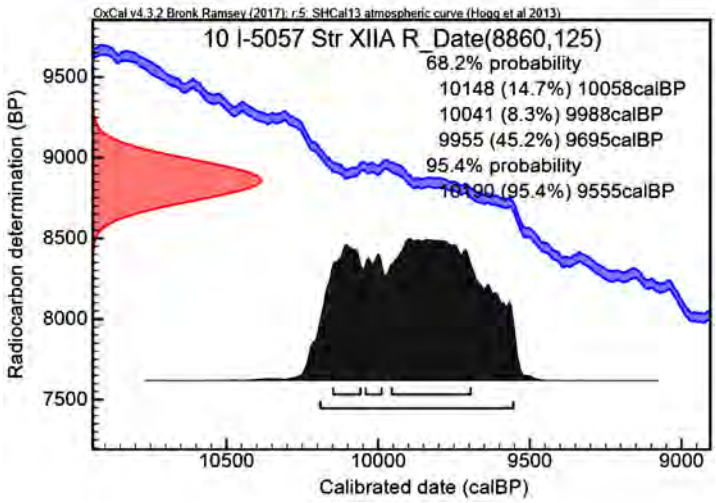

Figure 8. Plot showing the date of the sample I-5057 from XIIA strata as well as the 95.4% and 68.2% probability calibrated age ranges and the ShCal13 curve for the southern hemisphere.

3. Materials, Analysis and Observations

The analyzed collection is curated in the Museum of Archeology of the San Marcos University (Lima, Peru). Also, there are a few objects at the Environmental Archaeology Program of the Florida Museum of Natural History (FLMNH), Gainesville, Florida, USA. The study of the field-notes taken by MacNeish and his team at the Robert S. Peabody Institute of Archaeology (Andover, Massachusetts, USA) complemented this research. A total of 4052 human-made artifacts were studied and recorded whose distribution by strata is described in **Table 1**.

We processed the morpho-technological analysis according to several general typological guidelines (de Sonneville-Bordes & Perrot, 1956; Bordes, 1981; Piel-Desruisseaux, 1989; Merino, 1994; Inizan et al., 1995); the schemas were proposed explicitly for the Peruvian Andes (Bonavia, 1982, 1992; Chauchat, 1972, 1982; Lavallée et al., 1995), and other lithic analysts (e.g., Crabtree, 1972; Callahan, 1979; Andrefsky Jr., 2005; among others). Following is the list and a brief description of the tools' classes defined for this investigation.

A. Unifacial tools.

A.1. *Flakes with marginal retouch*. These are diverse kinds of flakes presenting small non-regular discontinuous, unifacial, bifacial, or alternating retouches, generally located at the distal portion and/or lateral edges (Bordes, 1981: p. 67).

A.2 *Denticulates*. Made on flake-blanks showing series of cut-outs or multiple-notched shapes as more or less regular indentations on one or more edges (Merino, 1994: p. 69).

A.3 *Unifaces*. Pieces reduced on one face generally having oval shapes, and generally plane-convex cross sections (Andrefsky Jr., 2005: p. 229).

A.4 *Side-scrapers*. Made on flakes with semi-abrupt continuous retouches modifying one or more edges, creating a straight, concave, or convex edge without cut-outs (Merino, 1994: p. 64; Piel-Desruisseaux, 1989: pp. 75-76).

Table 1. Lithic list discriminated by layers.

Lithic Typology Puente site			
Categories	Strata		
	XIV	XIII	XIIA
A. Unifacial tools			
A.1. Flakes with marginal retouch	-	11	4
A.2 Denticulates	-	2	-
A.3 Unifaces	-	2	-
A.4 Side-scrapers	-	3	-
A.5 End-scrapers	-	9	14
B. Bifacial artifacts			
B.1 Projectile points	-	14	1
B.2 Early bifacial stages and preforms	-	6	-
C. Pebble implements			
C.1 Hammer-stones	-	1	-
C.2 Manuports and ecofacts	-	4	2
D. Flaking waste			
D.1 Flakes and shatters	38	1754	2181
D.2 Cores	-	4	2
Total	38	1810	2204

A.5 *End-scrapers*. Generally made on different types of flakes that show a continuous non-abrupt retouching delineating a rounded or convex distal edge (Merino, 1994: p. 67; de Sonneville-Bordes & Perrot, 1956).

B. *Bifacial artefacts*.

B.1. *Projectile points*. This is a pointed artefact that was hafted to a weapon, sometimes used to accomplish other functions such as a knife.

B.2. *Biface and preform*. Piece partially or totally flaked on both faces with shapes varying from roughly oval to the outlining of the desired product (Crabtree, 1972; Callahan, 1979; Nami, 1986, 2003, 2017).

C. *Implements and ecofacts*.

C.1. *Hammer-stones*. Oblong pebbles with impact marks on one of their ends, usually resulting from percussion (Crabtree, 1972; Callahan, 1979).

C.2. *Manuports and ecofacts*. Pebbles that were without use-wear or modification, but possibly transported to the site by a human intervention (Leakey, 1979; Sharer & Ashmore, 1979).

D. *Flaking waste*.

D.1. *Debitage*. Here we include the by-products resulting from the stone tool's manufacture, such as flakes and shatters (Andrefsky Jr., 2005; Leroi-Gourhan, 2005: p. 309).

D.2. *Cores*. Pieces resulting from blank obtaining for making stone tools

(Leroi-Gourhan, 2005: p. 792; Andrefsky Jr., 2005: pp. 81-82).

Table 1 shows the list of artifacts by layers, and Figure 9(a) & Figure 9(b) gives the origin, measurements, raw materials, tool class, and other data. Figure 10

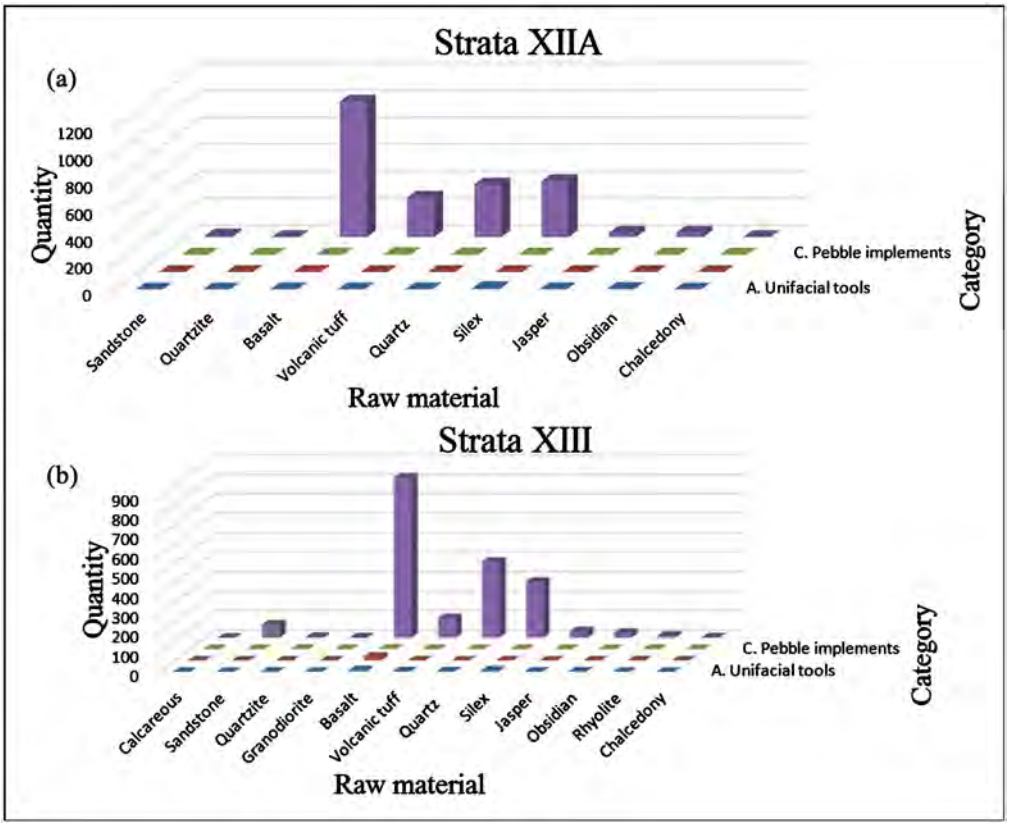

Figure 9. Raw materials' distribution versus debitage and lithic categories from strata XIIA (a) and XIII (b).

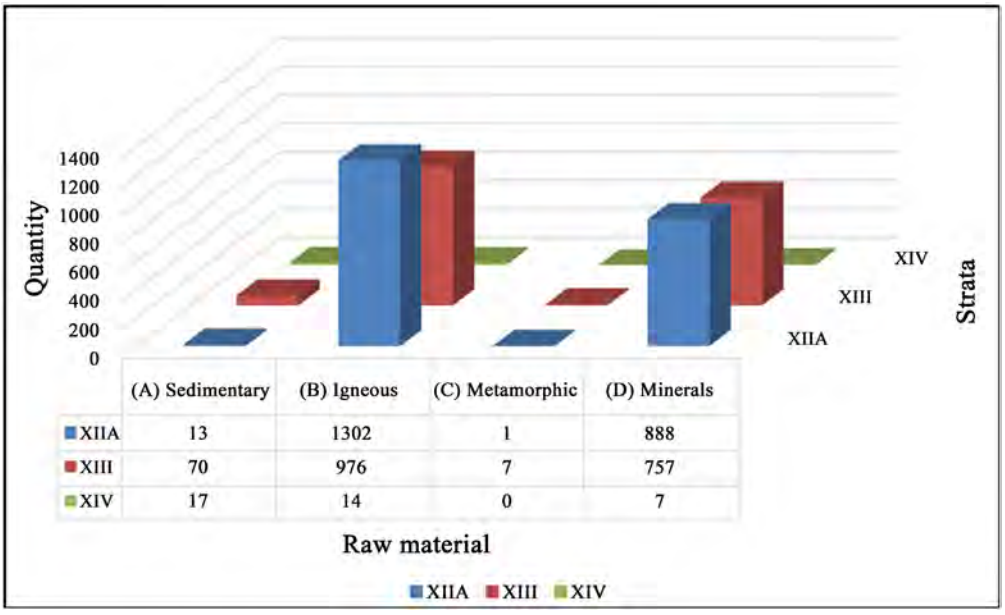

	(A) Sedimentary	(B) Igneous	(C) Metamorphic	(D) Minerals
XIIA	13	1302	1	888
XIII	70	976	7	757
XIV	17	14	0	7

Figure 10. Raw materials' quantity discriminated by group and strata.

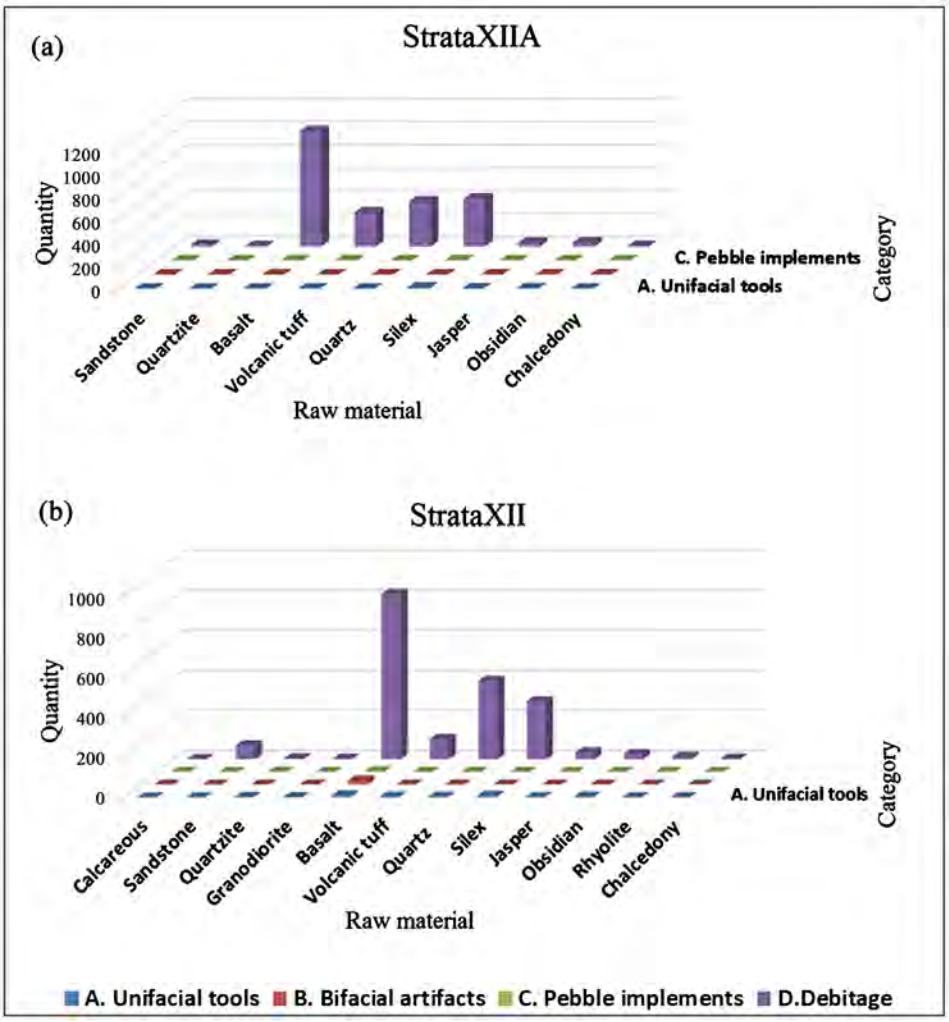

Figure 11. Raw materials' distribution versus lithic categories from strata XIIA (a) and XIII (b).

and Figure 11 illustrate the most notable analyzed artifacts. Using experimental and ethno-archaeological research, we can make a variety of observations of the stone tool technology present in the lowest layers of the rock-shelter.

Guided by geologist C. Toledo, the raw materials were macroscopically examined using a 10× to 35× magnifying glass, and sometimes a hand-held microscope up to 250×. They were grouped as follows: Group A, Sedimentary, made up of sandstones and calcareous materials; Group B, Igneous, including granodiorite, granite, andesite, rhyolite, basalt, volcanic tuff, and gabbro; Group C, Metamorphic, among which stand out quartzite and anthracite; finally, Group D encompasses silica-based minerals, among which we include the flint-like materials (silex or chert), jasper, obsidian, quartz, and chalcedony (Dana, 1998).

Figures 9-11 show that groups B and D are the most abundant material in layers XIIA to XIV. The former is available in the seasonal creek located at ~50 m from the site. Its ravines constitute a secondary source (Luedtke, 1979) containing pebbles of quartzite, basalt, granodiorite, rhyolite, and volcanic tuff. The sources of some the Group D rocks are still unknown. However, several natural

deposits at Quispisisa and Puzolana, located at Ayacucho, are the best-documented and closest obsidian supply (Matsumoto et al., 2018; Giesso et al., 2020). A few obsidian samples (n = 4) from layers XII-XIII analyzed using XRF and NAA methods showed that two artifacts come from Quispisisa, and another two from Puzolana (Burger & Asaro, 1979, 1993: table 12; Burger & Glascock, 2000: pp. 292-293).

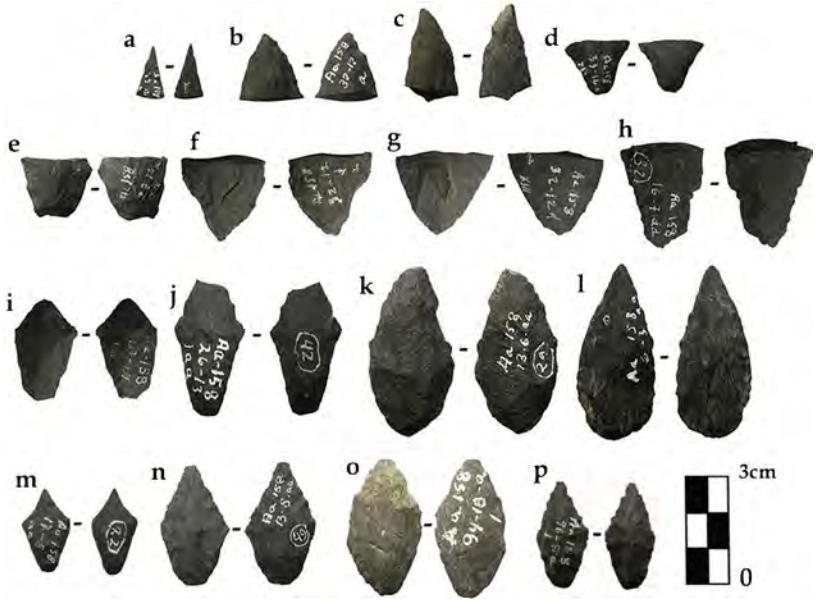

Figure 12. Projectile points in different condition recovered in stratum XIIA (p) and XIII (a)-(o).

From levels XIIA–XIII comes one rhomboidal point, and three complete pieces showing lanceolate, bi-pointed, and rhomboidal shapes, tips, and basal portions fractured by impact (Newcomer, 1980), some with contracting stems (**Figure 12**). Although, some specimens exhibit short retouches allowing the observation of the flake-blank' (**Figures 12(e)-(h)**), most were finished by covering pressure flake-scars applied with a non-regular pattern (**Figures 12(m)-(p)**). As a typical behavior in bifacial implements' life trajectories, they were resharpened and reworked (e.g. Ahler, 1971). This is detectable when the blade form and symmetry are highly modified; retouches show a change in the remaining original pattern; the borders are strongly rounded or concave (Callahan, 1981), or do not have enough mass to continue the task. This kind of repair was generally made when the piece was hafted (Nami, 2013). Considering coeval lanceolate points with little or no resharpening (e.g., Rick, 1983: fig. 44d-e), the specimens displayed in **Figure 12(i)**, **Figures 12(j)-(l)** show intense rejuvenation. This fact is also visible in other Peruvian exemplars (e.g., Lynch, 1967: fig. 2a-h; Rick, 1983: fig. 44k-l, n-o). In addition to the discarded points, the remaining five bifacial pieces from layer XIII are early manufacturing stages rejected by flaking failures, such as hinges, steps, and an oblique fracture (**Figures 13(a)-(e)**; Callahan, 1979).

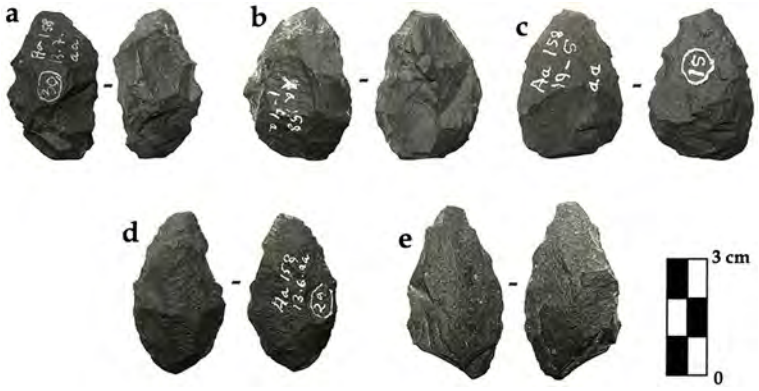

Figure 13. Bifacial stages of manufacture from layer XIII.

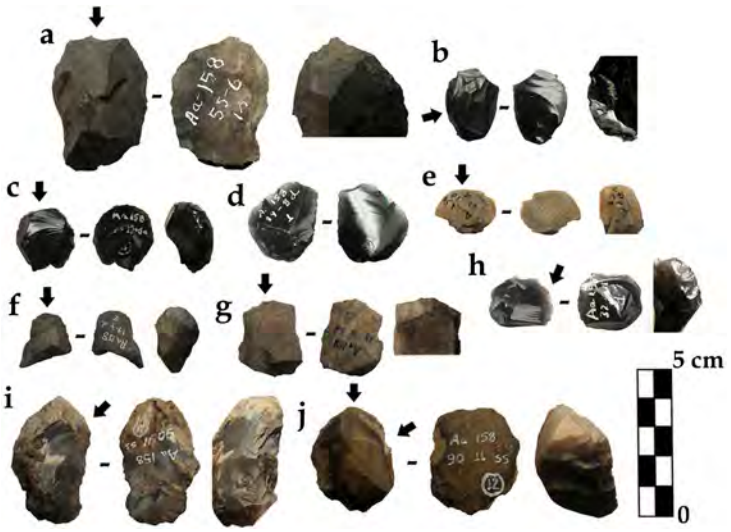

Figure 14. Illustrative examples of unifacial tools from layer XIIA. The arrows in this and the next figure point to the edges' close-up picture depicted on the right of each specimen.

Besides side-scrapers and denticulates (**Figure 14((b), (h)-(j))**), most unifacial tools are the end-scrapers (**Figure 14((a), (c), (e), (f))**) and flakes with marginal retouch (**Figures 14((d), (g))**). Special care was taken with the latter because pieces with a sharply acute edge-angle, their retouches, may result from a natural edge use (Bordes, 1981), unintentionally originated by trampling, and another kind of taphonomic processes (Eren et al., 2011). The unifaces were mostly made using tertiary flake blanks (**Figures 14((a)-(h), (j))**; **Figures 15(u)-(w)**; **Figure 16(u)**, **Figures 14((y), (z))**) and a few with primary (**Figures 15((i), (t))**; **Figure 16(k')**) and secondary flakes (**Figure 14(i)**; **Figures 15((g), (h), (j)-(q), (s), (u)-(w))**). They were obtained by hard hammer (**Figures 15((g), (i), (j))**; **Figures 16(h), (i), (n), 16(p)-(t))**), or soft direct percussion flaking, exhibiting flat and diffuse force application bulbs and lips (**Figures 15((b)-(e), (h))**; **Figure 16((e), (f), (j), (m), (o), (u)-(w))**), depending on the material, as experimentally revealed (Crabtree, 1972; Callahan, 1979; Nami, 2015, 2017). The retouches vary from short regular and irregular parallel (**Figures 15(u)-(w)**) to scalariform (**Figure 15(p)**). When a flake's dorsal and ventral faces are visible, most re-

touches are direct (**Figures 14(a)-(j)**; **Figures 15((e)-(i), (k), (n)-(o), (q)-(t))**; **Figures 16((l)-(x), (i')-(l'))**), and inverse in a few cases (**Figure 15(p)**). It is highly probable that final shaping was performed by merely retouching a blank's edges using the same technique, but with another variant and/or holding position, and using soft or semi-soft hammer-stones Due to their small dimensions, most of the unifacial tools might have been used hafted (references in Shott, 1995).

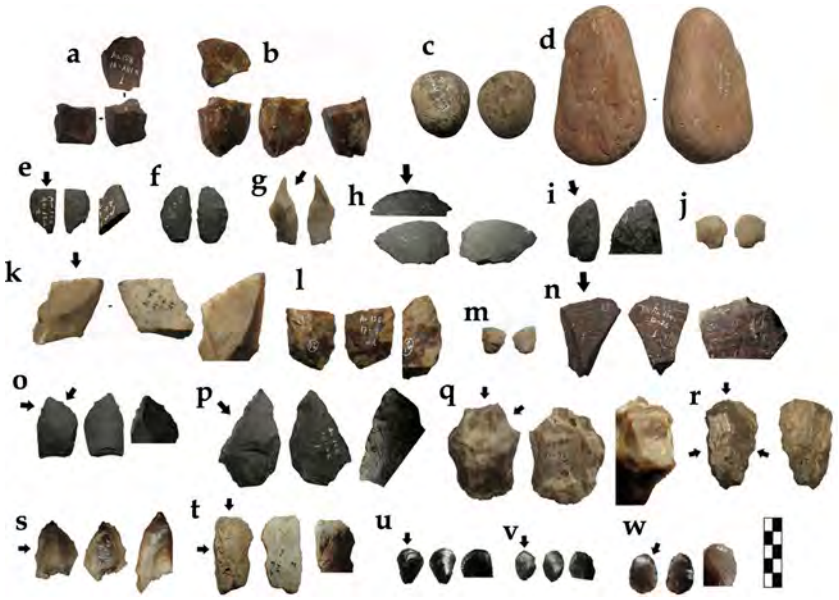

Figure 15. Cores ((a), (b)), ecofacts ((c), (d)) and unifacial tools (e)-(w) from layer XIII.

The lithic waste represents the majority of the remains of the scrutinized sample. The **Table 2** describes the materials in terms of formation, origin, workability, hardness, using a scale ranging from "bad" to "excellent" according to the degree of workability of the rocks (Nami, 2015), and their potential employment in different flaking strategies and techniques (Tixier et al., 1980). **Table 3** depicts its dimensional average means by strata.

The cores varied from orthogonal, trapezoidal, and bifacial shapes (**Figure 15(a)**, **Figure 15(b)**; **Figures 16((n), (m')-(o'))**. The manuports and ecofacts consisted of a hammer-stone and pebbles recovered at the nearby Wichqana creek, whose shapes range from circular, elliptical, and oblong (**Figure 15(c)**, **Figure 15(d)**). The former shows percussion marks on one of its sharpest sides, while the latter has soot traces, probably related to some combustion phenomena (**Figure 15(c)**). Besides the aforementioned cores, the drawing depicted in **Figure 16** exemplifies a few laminar flakes (**Figures 16(a)-(d)**), pressure flake debitage (**Figures 16(f)-(i)**), diverse kinds of unifacial tools as well their fragmented edges (e.g. **Figures 16((j)-(m), (r)-(x), (f'), (j'), (l'))**).

We identified twenty-six bone remains from the analyzed strata, six modified by grinding and polishing, and twenty small fragments altered by fire. As seen in **Figure 17** from XIIA come two well-made awls and a part of a polish specimen (**Figure 17(a)** & **Figure 17(b)**), previously reported as "Split and Conical awls"

Table 2. List of lithic materials reported in this paper.

Variety of Lithic Materials	Rock	Origin	Hardness*	Range	Typology+	Strategies and techniques	Figure
Sedimentary	Calcareous	local	3	R	D.1	PF, PrF	-
	Sandstone	local	3	R	D.1	PF, PrF	-
Metamorphic	Quartzite	local	7	R-B	A.1, C.1, D.1	PF	Figure 15(d), Figure 15(e); Figure 16(q)
Igneous intrusive	Granodiorite	Local, Wichqana creek	7	R-B	D.1	PF	-
Igneous volcanic	Basalt	Local, Wichqana creek	4.8 - 6.5	R-G	A.1, C.2,A.4, A.5, B.1, B.2, D.1, D.2	PF, PrF, BR	Figures 12(a)-(p); Figures 13(a)-(e); Figure 14(f); Figures 15((c), (f), (h)-(i), (o)-(p)); Figures 16((b), (e), (h), (m), (r), (w), (a'), (d'), (g'), (i'), (k'))
	Volcanic tuff	Local, Wichqana creek	7	R-G	A.1, A.3, A.5, C.2, D.1, D.2	PF, PrF	Figures 15((a), (n)), Figures 16((d), (j), (s), (j'), (l'), (m'), (n'))
	Rhyolite	local	6.5 - 7	R—G	C.2, D.1, D.2	PF	Figure 16(n)
Minerals	Quartz	not determinated	7	G-E	A.1, A.5, A.2, D.1, D.2	PF, PrF	Figures 15((g), (j), (m), (q)), Figures 16((g), (k), (p), (v), (c'))
	Silex or chert	not determinated	7	G-E	A.1, A.2, A.3, A.5, D.1, D.2	PF, PrF	Figures 14((e), (g), (i), (j)); Figures 15((b), (k), (l), (r)-(t)); Figures 16((a), (c), (f), (l), (o), (t), (b'), (e'), (f'), (h'), (o'))
	Jasper	not determinated	6.5 - 7	G-E	A.1, A.4, D.1	PF, PrF	Figure 14(a); Figure 16(x)
	Obsidian	possible Puzolana or Quispisisa	5 - 7	G-E	A.1, A.5, D.1	PF, PrF	Figures 14((b)-(d, (h)); Figures 15(u)-(w), Figures 16((u), (y)-(z))
	Chalcedony	not determinated	7	G-E	D.1	PF, PrF	Figure 16(i)

Abbreviations: *Mohs scale. R: Regular, B: Bad, G: Good, E: Excellent. +: Typology code according Table 1. PF: Percussion flaking, PrF: Pressure flaking, BR: Bifacial reduction.

Table 3. Average measurements by artefacts classes.

Artefacts' classes	Strata														
	XIV					XIII					XIIA				
	Q	L	W	T	We	Q	L	W	T	We	Q	L	W	T	We
A.1. Flakes with marginal retouch	-	-	-	-	-	11	32.7	31.6	9.2	8.6	4	26.7	22.7	8.75	7.05
A.2 Denticulates	-	-	-	-	-	2	42	42	19	38.15	-	-	-	-	-
A.3 Unifaces	-	-	-	-	-	2	46.5	27.5	11.5	17.9	-	-	-	-	-
A.4 Side-scrapers	-	-	-	-	-	3	36	42	6.6	10.6	-	-	-	-	-
A.5 End-scrapers	-	-	-	-	-	9	29	22.8	9.5	8.24	14	29	26.8	12.21	12.15
B.1 Projectile points	-	-	-	-	-	14	24.2	19.2	557	2.6	1	28	15	5	1.7
B.2 Early bifacial stages and preforms	-	-	-	-	-	6	39.8	22.1	8.1	5.91	-	-	-	-	-
C.1 Hammer-stones	-	-	-	-	-	1	97	70	41	417.2	-	-	-	-	-
C.2 Manuports and ecofacts	-	-	-	-	-	4	63.2	44.5	30.5	113.2	2	98	81	63	734.9
D.1 Flakes and shatters	36	12.85	15.75	4	8.6	1754	13.3	14.3	4	1	2181	12	13	3	0.5
D.2 Cores	-	-	-	-	-	4	42.25	41.25	24	106.75	2	57	44.5	25.5	65.6

Q: Total quantity; L: Length; W: Width, T: Thickness (mm); We: Weight (gr).

Figure 16. Illustrative specimens of the analysed sample from layers XIIA (a)-(c) and XIII (d)-(o').

Figure 17. Remarkable bone objects from layers XIIA. (a) Split bone awl; (b) polish bone fragment; (c) conical bone awls.

Figure 18. Burned mammal sawed phalange.

Figure 19. Bone specimens from level XIII. (a) unclassified fragment; (b) pierced base netting needles; (c)-(e) triangular pendants; (f)-(h) fragmented objects.

and "Polish bone fragment" (MacNeish et al., 1980: fig. 8-13). From the profile of grid S9, in the FLMNH collections, there is one small epiphysis of a burned phalange (EA 01180738) weighting 0.2 g with sawing marks at one of its ends that looks like score and snap debitage from making a bone good (**Figure 18**). From layer XIII comes ten burned specimens; seven are well-made objects, while the remaining are small bone fragments. Remarkable pieces displayed in **Figure 19(b)-(e)** were classified as *"Pierced Base netting needles"* and *"Triangular Pendants"* (MacNeish et al., 1980: pp. 317-318, fig. 8-14). The latter was well-made by grinding on some abrasive material that left striae visible to the naked eye; finally, polishing was employed to finishing them.

4. Results and Interpretation

The shaped tools from layers XIIA–XIII shows morpho-technological similarities. Hence, they belong to Early Holocene hunter-gatherers living at the ~≥10.3 - 9.5 calibrated kya. The low frequency of lithic artefacts in layer XIV may have come from the upper layer, or they testify the presence of an older occupation.

Given the lithic waste's dimensional ranges, these are results from manufacturing tools, suggesting that it was an important activity performed at the site. They are mainly by-products from bifacial thinning, final shaping, and rejuvenation of uni- or bifacial instruments. In this endeavour, the knappers may have used hard-percussion flaking, but also soft-precursors according to the reduction technique (Flenniken 1984: p. 191) and step in the process (Callahan, 1979; Nami, 2017). Due to their size and punctiform striking platforms, some of the smallest flakes result by the use of pressure flaking (Andrefsky Jr., 2005; Nami, 2017). The most used materials were local basalt, followed by silex and jasper, the quarries of which are still unknown. The obsidian comes from the Quispisisa and Puzolana sources. The former is located at ~120 km distance from the Puente site, while the latter is in the site's vicinity at ~10 - 15 km (Burger & Glascock, 2000; Giesso et al., 2020).

One of the activities performed at layers XIIA–XIII was the weaponry repairing, possibly replacing exhausted and broken points for new ones. Although there are entire specimens, most are rejuvenated and fractured pieces, either tips or basal portions. The finding of extremely resharpened points, fractured bases, and early bifacial stages of reduction suggest this fact. In addition to waste, there is a profusion of debitage that evidences final shaping by pressure flaking. Under the actualistic baseline generated by replicative experiments on similar materials to those recovered at Puente especially basalt-, and other rocks (Callahan, 1979; Nami, 1986, 2015, 2017), it is possible to suggest that the waste's flakes resulted from hard and soft percussion flaking. This fact is consistent with that of some of the early stages bifaces, which showed flake-scars with sharp ridges and profound concave initiations remaining from pronounced bulbs of percussion (**Figure 13**). Others show flat initiations resulting from the flakes' detachment with diffuse bulbs (Crabtree, 1972; Callahan, 1979; Nami, 1986, 2017). Coincidently, much debitage displays thin, angular flakes with multidirectional ridges and curved longitudinal cross section. In addition, they show narrow and abraded faceted—or filiform—platforms, and sometimes lips. Experiments making similar lanceolate pieces (Nami, 1988-1990) suggest that the rejected bifacial specimens are early manufacturing stages and preforms. On these bases, their flake-scars' features indicate that they were probably flaked with hammer-stones (**Figures 13(a)-(e)**) and organic precursors, possibly antler or bone (**Figures 12(i)-(p)**). The small sample from layer XIV is debitage mainly represented by diverse small tertiary flakes. By their characteristics, they may result from bifacial thinning stages and final shaping (Callahan, 1979; Nami, 1986, 2017; Whittaker & Kaldahl, 2001; Purtill, 2012).

Random multidirectional flakes extremely reduced the cores, suggesting the materials' maximization. The pebbles and cobbles in traditional technologies generally are multipurpose implements (De Beaune, 1989). One was used as a hammer-stone, while the ecofacts were probably employed in diverse ways. Those with soot traces were perhaps related to some combustion or culinary action.

5. Discussion and Conclusion

In summary, the raw material procurement in general was local. However, the presence of obsidian from Quispisisa verified that, since the terminal Pleistocene, the Andean societies made long-distance interregional movements or exchanges (Burger & Asaro, 1993; Matsumoto et al., 2018). Similarly, its use for making stone tools by the earliest hunter-gatherer occupations at Ayacucho was also recorded in the Pikimachay cave, and the Jaywamachay rock shelter (García Cook et al., 1981; Yataco Capcha & Nami, 2016).

The analysed shaped artefacts show small sizes with standardized forms. The projectile points' morphology and unifacial tools agree with those registered in early Holocene sites in the Central and Southern Andes: in Peru at Lauricocha (Cardich, 1958: fig. 11a-f; fig. 12, fig. 25-27; Cardich, 1964: fig. 79-86); Quisqui Puncu (Lynch, 1967), Guitarrero (Lynch, 1980: fig. 9.1: c-d, h-j; fig. 9.2: o; fig. 9.3: a, h, j); Pachamachay (Rick, 1980: fig.6 .13-6.14, fig. 7.2-7.11; Rick, 1983: fig. 44a-o; fig. 45g-h); Uchkumachay (Kaulicke, 1999: pp. 307-324 fig.3-12); Telarmachay and Quebrada de los Burros (Lavallée, 1995: pp. 127-129; Lavallée & Julien, 2012: pp. 223-224); Tres Ventanas, Kiqche sites (Chauchat, 1972: pp. 126-132, fig, 4-5); and Toquepala (Ravines, 1972: pp. 133-184), as well many other places (e.g. Sandweiss & Rademaker, 2011); Chile (Osorio et al., 2011), Bolivia (Aldenderfer, 1998: fig. 6.24; Lizarraga-Mehringer, 2000: pp. 124-138, 156-161; Rivera Casanovas & Calla Maldonado, 2011: fig. 8a-p), and Argentina (González, 1960; Gradín, 1984; Fernández, 1988-1990).

In Ayacucho, diverse projectile point types were defined based on their morphological variations (MacNeish et al., 1983: pp. 50-57). Several reflect different shapes with little or no resharpening (MacNeish et al., 1980: pp. 53-64). However, some of these might result from the rejuvenation of the same ones, and the points from layers XIIA–XIII reflect this case. It is worth mentioning that in the lower levels of Guitarrero, Jaywamachay rock shelter and Pikimachay caves, with a similar chronology, the case of Guitarrero Cave is special, because the lithic artefacts were associated with well-preserved remains of wood, bone, antler, twine, and vegetable fibre textiles (Lynch & Kennedy, 1970: fig. 1). Like other hunter-gatherers in the world (Schier & Pollock, 2020), these elements suggest an early textile development in the Central Andes, almost coincident with the oldest evidence of Andean agriculture and the origin of the well-known sociocultural complexification in the Central Andes (Dillehay et al., 2007).

From a culture-history perspective, MacNeish and associates proposed a long regional sequence segmented in several phases according to their excavations in

the Ayacucho Basin, mostly named with traditional Quechua names, for instance Phases Puente Jaywa, Piki, Chihua, Cachi, etc. (García Cook et al., 1981: pp. 199-266). The archaeological vestiges of layers XIIA-XIII and XIV were attributed as belonging to some of the oldest phases called "Jaywa" and "El Puente" (García Cook et al., 1981: pp. 87-94; MacNeish et al., 1983: pp. 50-55). From our perspective, the findings from levels XIIA–XIII belong to Early Holocene hunter-gatherers. Those from layer XIV may come from the upper layer, or testify a short occupation event of an older Paleoindian group living at the time of the Younger Dryas at ~13.0 - 12.2 calibrated kya. In general, low remains' densities characterized some early South American records (e.g. Politis et al., 2019). From that period, the Jaywamachay rock shelter, and other Peruvian sites yielded "fishtail" points (e.g., MacNeish et al., 1980; García Cook et al., 1981; Rademaker et al., 2014; Maggard, 2015; Yataco Capcha & Nami, 2016). Widely distributed from southern Mexico to southernmost South America, this iconic Paleoindian artifact evidences the Andean/Pacific path followed by the foragers intervening in the colonization of South America (Nami, 2021).

Acknowledgements

We are deeply indebted to: Dr. Ryan Wheeler, director of the Robert S. Peabody Institute of Archaeology; Dr. Jorge Silva, director of the Museo de Arqueología y Antropología de la Universidad Nacional Mayor de San Marcos, and César Franco, director of the Centro Cultural de San Marcos, Lima-Perú; Florida State Museum for their cooperation during the study of the materials and field notes of the "Ayacucho-Huanta Project", C. Toledo (geologist of the Universidad Nacional Mayor de San Marcos. Lima-Perú) for his invaluable help in classifying the rocks. Ryan Wheeler provided invaluable editing of an early draft of this paper.

Conflicts of Interest

The authors declare no conflicts of interest regarding the publication of this paper.

References

Ahler, S. (1971). *Projectile Point Form and Function at Rodgers Shelter.* Columbia, MO: College of Arts and Science, University of Missouri.

Aldenderfer, M. (1998). *Montane Foragers. Asana and the South-Central Andean Archaic*. Iowa City, IA: University of Iowa Press. https://doi.org/10.2307/j.ctt20q1wq5

Andrefsky Jr., W. (2005). *Lithics: Macroscopic Approaches to Analysis*. Cambridge: Cambridge University Press. https://doi.org/10.1017/CBO9780511810244

Bonavia, D. (1982). *Precerámico peruano, Los Gavilanes: Mar, Desierto y Oasis en la Historia del Hombre*. Lima: COFIDE-Instituto Arqueológico Alemán.

Bonavia, D. (1992). Tipología Lítica Tentativa para el Precerámico Final de la Costa Central y Septentrional del Perú. In D. Bonavia (Ed.), *Estudios de arqueología Peruana* (pp. 83-97). Lima: APFCS-FOMCIENCIAS.

Bordes, F. (1981). *Typologie du Paleolitique Ancien et Moyen*. Bourdeux: Delmas. Publications de I'nstitut de Préhistoire de l'université de Bourdeux-CNRS.

Bronk Ramsey, C., & Lee, S. (2013). Recent and Planned Developments of the Program OxCal. *Radiocarbon, 55,* 720-730. https://doi.org/10.1017/S0033822200057878

Burger, R., & Asaro, F. (1979). Análisis de rasgos significativos en la obsidiana de los Andes Centrales. *Revista del Museo Nacional, XLIII,* 281-325.

Burger, R., & Asaro, F. (1993). *La distribución y procedencia de artefactos de obsidiana durante el Periodo Inicial y Horizonte Temprano. Emergencia de la civilización en los Andes ensayos de interpretación*. Lima: Universidad Nacional Mayor de San Marcos.

Burger, R., & Glascock, M. (2000). Locating the Quispisisa Obsidian Source in the Department of Ayacucho, Peru. *Latin American Antiquity, 11,* 258-268.

Callahan, E. (1979). The Basics of Biface Knapping in the Eastern Fluted Point Tradition. A Manual for Flintknappers and Lithic Analysts. *Archaeology of Eastern North America, 7,* 1-180.

Callahan, E. (1981). *Pamunkey Housebuilding: An Experimental Study of Late Woodland Construction Technology in the Powhatan Confederacy*. Ph.D. Thesis, Washington DC: Catholic University of America.

Cardich A. (1958). *Los Yacimientos de Lauricocha. Nuevas interpretaciones de la Prehistoria Peruana. Estudia Praehistórica I*. Buenos Aires: Centro argentino de Estudios Prehistóricos.

Cardich A. (1964). *Lauricocha. Fundamentos para una prehistoria de los Andes Centrales. Estudia Prehistórica III*. Buenos Aires: Centro argentino de Estudios Prehistóricos.

Chauchat, C. (1972). Ensayo de Tipología Lítica del Precerámico Peruano. *Revista del Museo Nacional, XXVIII,* 125-132.

Chauchat, C. (1982). *Le Paijanien du Desert de Cupisnique. Recherches Sur l'Occupation Préhistorique de la Côte Nord du Pérou au Début de l'Holocène*. Thése de Doctorat d'État ès Sciences, Burdeaux: Université de Bordeaux.

Crabtree, D. (1972). *An Introduction to Flintworking*. Pocatello, Occasional Papers of the Idaho State University Museum.

Dana, J. D. (1998). *Manual of Mineralogy* (21st ed.). New York: John Wiley and Sons.

de Beaune, S. A. (1989). Exemple ethnographique de l'usage pluri-fonctionnel d'un galet de quartz. *Bulletin de la Société Préhistorique Française, 86,* 61-64. https://doi.org/10.3406/bspf.1989.9363

de Sonneville-Bordes, D., & Perrot, J. (1956). Lexique Typologique du Paleolithique Superior. *Bulletin de la Société Préhistorique Française, 53,* 327-335. https://doi.org/10.3406/bspf.1956.3374

Dillehay, T. (1985). A Regional Perspective of Preceramic Times in the central Andes. *Reviews in Anthropology, 12,* 193-205. https://doi.org/10.1080/00988157.1985.9977731

Dillehay, T., Rossen, J., Andres, T., & Williams, D. (2007). Preceramic Adoption of Peanut, Squash, and Cotton in Northern Peru. *Science, 316,* 1890-1893. https://doi.org/10.1126/science.1141395

Eren, M. I., Boehm, A., Morgan, B. M., Anderson, R., & Andrews, B. (2011). Flaked Stone Taphonomy: A Controlled Experimental Study of the Effects of Sediment Consolidation on Flake Edge Morphology. *Journal of Taphonomy, 9,* 201-217.

Fernández, J. (1988-1990). La cueva de Haichol: Arqueología de los pinares cordilleranos del Neuquén. *Anales de Arqueología y Etnología, 43-45*.

Flenniken, J. J. (1984). The Past, Present, and Future of Flintknapping: An Anthropological Perspective. *Annual Review of Anthropology, 13,* 187-203.

https://doi.org/10.1146/annurev.an.13.100184.001155

García Cook, A., & MacNeish, R. S. (1981). Stratigraphy of Puente, Ac158. In R. S. MacNeish, A. Garcia Cook, L. Lumbreras, R. K. Vierra, & A. Nelken-Terner (Eds.), *Prehistory of the Ayacucho Basin, Peru. Vol. II, Excavations and Chronology* (pp. 80-112). Ann Arbor, MI: University of Michigan Press. https://doi.org/10.3998/mpub.9690722

Giesso, M., Nami, H. G., Yataco Capcha, J. J., Glascock, M. D., & MacDonald, B. L. (2020). XRF Obsidian Analysis from Ayacucho Basin, Huamanga Province, Southeastern Peru. *Archaeometry, 62,* 215-231. https://doi.org/10.1111/arcm.12529

González, A. R. (1960). La estratigrafía de la gruta de Intihuasi, (Prov. de San Luis, RA) y sus relaciones con otros sitios precerámicos de Sudamérica. *Revista del Instituto de Antropología,* 5-296.

Gradín, C. J. (1984). *Investigaciones Arqueológicas en Casa de Piedra*. La Pampa: Dirección General y Ente Ejecutivo Casa de Piedra.

Hogg, A. G., Hua, Q., Blackwell, P. G., Niu, M., Buck, C. E., Guilderson, T. P., Heaton, T. J., Palmer, G., Reimer, P. J., Reimer, R. W., Turney, C. S., & Zimmerman, S. R. H. (2013). SHCal13 Southern Hemisphere Calibration, 0 - 50,000 Years cal BP. *Radiocarbon, 55,* 1889-1903. https://doi.org/10.2458/azu_js_rc.55.16783

Inizan, M. L., Reduron, M., Roche, H., & Tixier, J. (1995). *Technologie de la Pierre Taillée*. Meudon: CREP.

Kaulicke, P. (1999). Contribuciones hacia la cronología del Periodo Arcaico en las punas de Junín. *Boletín de Arqueología PUCP, 3,* 307-324.

Lavallée, D., & Julien, M. (2012). *Prehistoria de la Costa Extremo-Sur del Perú. Los Pescadores arcaicos de la Quebrada de los Burros (10,000-7,000 a.P.)*. Lima: Instituto Francés de Estudios Andinos y Fondo Editorial de la Pontificia Universidad Católica del Perú. https://doi.org/10.4000/books.ifea.7519

Lavallée, D., Julien, M., Wheeler, J., & Karlin, C. (1995). *Telarmachay: Cazadores y Pastores Prehistóricos de los Andes*. Lima: IFEA. https://doi.org/10.4000/books.ifea.10363

Leakey, M. (1979). *Olduvai Gorge*. London: Book Club Associates.

Leroi-Gourhan, A. (2005). *Dictionnaire de la Préhistoire*. Paris: Quadrige/PUF.

Lizarraga-Mehringer, Y. (2000). *Viscachani y el Precerámico de Bolivia*. PhD Thesis, Köln: Universität zu Köln.

Luedtke, B. (1979). The Identification of Sources of Chert Artifacts. *American Antiquity, 44,* 744-757. https://doi.org/10.2307/279116

Lynch, T. F. (1967). Quishqui Puncu: A Preceramic Site in Highland Peru. *Science, 158,* 780-783. https://doi.org/10.1126/science.158.3802.780

Lynch, T. F. (1980). *Guitarrero Cave. Early Man in the Andes*. Cambridge, MA: Academic Press.

Lynch, T. F., & Kennedy, K. R. (1970). Early Human Cultural and Skeletal Remains from Guitarrero Cave, Northern Peru. *Science, 169,* 1307-1309. https://doi.org/10.1126/science.169.3952.1307

MacNeish, R. S. (1969). *First Annual Report of the Ayacucho Archaeological-Botanical Project*. Andover, MA: Robert S. Peabody Found for Archaeology.

MacNeish, R. S. (1981). Synthesis and Conclusions. In R. S. MacNeish, A. Garcia Cook, L. Lumbreras, R. K, Vierra, & A. Nelken-Terner (Eds.), *Prehistory of the Ayacucho Basin, Peru. Vol. II, Excavations and Chronology* (pp. 199-257). Ann Arbor, MI: University of Michigan Press. https://doi.org/10.3998/mpub.9690722.

MacNeish, R. S., Vierra, R. K., & García Cook, A. (1983). The Preceramic Way of Live in the Humid Wooland Ecozone. In R. S. MacNeish, A. Garcia Cook, L. Lumbreras, R. K, Vierra, & A. Nelken-Terner (Eds.), *Prehistory of the Ayacucho Basin, Peru. Vol. II, Excavations and Chronology* (pp. 188-218). Ann Arbor, MI: University of Michigan Press.

MacNeish, R. S., Vierra, R. K., Nelken-Terner, A., & García Cook, A. (1970). *Second Annual Report of the Ayacucho Archaeological-Botanical Project*. Andover, MA: Robert S. Peabody Found for Archaeology.

MacNeish, R. S., Vierra, R. K., Nelken-Terner, A., & Phagan, C. J. (1980). *Prehistory of the Ayacucho Basin, Peru. Vol. III, Nonceramic Artifacts*. Ann Arbor, MI: University of Michigan Press. https://doi.org/10.3998/mpub.9690719

Maggard, G. J. (2015). The El Palto Phase of Northern Peru: Cultural Diversity in the Late Pleistocene-Early Holocene. *Chungara, 47,* 25-40. https://doi.org/10.4067/S0717-73562015005000009

Matsumoto, Y., Nesbitt, J., Glascock, M., Cavero Palomino, Y., & Burger, R. (2018). Interregional Obsidian Exchange during the Late Initial Period and Early Horizon: New Perspectives from Campanayuq Rumi, Peru. *Latin American Antiquity, 29,* 44-63. https://doi.org/10.1017/laq.2017.64

Merino, J. M. (1994). *Tipología Lítica.* Tercera Edición. Munibe: Centro de Estudios Aranzadi.

Nami, H. G. (1986). *Experimentos para el estudio de la tecnología bifacial de las ocupaciones tardías en el extremo sur de la Patagonia Continental*. Buenos Aires: PREP: Informes de Investigación (Consejo Nacional de Investigaciones Científicas y Técnicas), 5.

Nami, H. G. (1988-1990). Simulación y réplica de las puntas de proyectil. La Cueva de Haichol. Arqueología de los pinares cordilleranos del Neuquén. *Anales de Arqueología y Etnología, 43/45,* 227-241.

Nami, H. G. (2003). Experimentos para explorar la secuencia de reducción Fell de la Patagonia Austral. *Magallania, 30,* 107-138.

Nami, H. G. (2013). Archaeology, Paleoindian Research and Lithic Technology in the Middle Negro River, Central Uruguay. *Archaeological Discovery, 1,* 1-22. https://doi.org/10.4236/ad.2013.11001

Nami, H. G. (2015). Experimental Observations on Some Non-Optimal Materials from Southern South America. *Lithic Technology, 40,* 128-146. https://doi.org/10.1179/2051618515Y.0000000004

Nami, H. G. (2017). Exploring the Manufacture of Bifacial Stone Tools from the Middle Rio Negro Basin, Uruguay: An Experimental Approach. *Ethnoarchaeology, 9,* 53-80. https://doi.org/10.1080/19442890.2017.1286757

Nami, H. G. (2021). Fishtailed Projectile Points in the Americas: Remarks and Hypotheses on the Peopling of Northern South America and Beyond. *Quaternary International, 578,* 47-72. https://doi.org/10.1016/j.quaint.2020.06.004

Newcomer, M. (1980). Savoir utiliser les outils préhistoriques. *Dossiers de l'Archéologie, 46,* 18-23.

Osorio, D., Jackson, D., Ugalde, P. C., Latorre, C., De Pol-Holz, R., & Santoro, C. M. (2011). Hakenasa Cave and Its Relevance for the Peopling of the Southern Andean Altiplano. *Antiquity, 85,* 1194-1208. https://doi.org/10.1017/S0003598X00062001

Piel-Desruisseaux, J. L. (1989). *Instrumental prehistórico forma fabricación utilización*. Barcelona: Masson.

Politis, G. G., Messineo, P. G., Stafford Jr., T. W., & Lindsey, E. L. (2019). Campo La-

borde: A Late Pleistocene Giant Ground Sloth Kill and Butchering Site in the Pampas. *Science Advances, 5,* eaau4546.

Purtill, M. (2012). *A Persistent Place: A Landscape Approach to the Prehistoric Archaeology of the Greenlee Tract*. Cincinnati, OH: Southern Ohio Gray & Pape, Inc.

Rademaker, K., Hodgins, G., Moore, K., Zarrillo, S., Miller, C., Bromley, G. R. M., Leach, P., Reid, D. A., Yépez Álvarez, W., & Sandweiss, D. H. (2014). Paleoindian Settlement of the High-Altitude Peruvian Andes. *Science, 346,* 466-469. https://doi.org/10.1126/science.1258260

Ravines, R. (1972). Secuencia y cambios en los artefactos líticos del sur del Perú. *Revista del Museo Nacional, XXVIII,* 133-184.

Rick J. (1980). *Prehistoric Hunters of The High Andes*. Cambridge, MA: Academic Press.

Rick J. (1983). *Cronología, clima y subsistencia en El Precerámico Peruano*. Lima: Ediciones INDEA. Instituto Andino de Estudios Arqueológicos.

Rivera Casanovas, C., & Calla Maldonado, S. (2011). Cazadores recolectores del Periodo Arcaico en los Valles y Serranias de la Región de San Lucas, Chuquisaca, Bolivia. *Chungara, 43,* 433-454. https://doi.org/10.4067/S0717-73562011000300007

Sandweiss, D. H., & Rademaker, K. M. (2011). El poblamiento del sur peruano: Costa y sierra. *Boletín de Arqueología PUCP, 15,* 275-293.

Schier, W., & Pollock, S. (2020). Introduction. In W. Schier, & S. Pollock (Eds.), *The Competition of Fibres: Early Textile Production in Western Asia, Southeast and Central Europe (10, 000-500 BC)* (pp. 1-3). Barnsley: Oxbow Books.

Sharer, R.J., & Ashmore, W. (1979). *Fundamentals of Archaeology*. Menlo Park, CA: Benjamin/Cummings Publishing Company.

Shott, M. J. (1995). How Much Is a Scraper? Curation, Use Rates, and the Formation of Scraper Assemblages. *Lithic Technology, 20,* 53-72.

Tixier, J., Inizan, M.-L., Roche, H., & Dauvois, M. (1980). *Prehistoire de la pierre taillée. I terminologie et technologie*. Meudon: C.R.E.P.

Whittaker, J. C., &Kaldahl, E. J. (2001). Where the Waste Went: A Knapper's Dump at Grassopper Pueblo. In W. Andrefsky Jr. (Ed.), *Debitage. Context, Form and Meaning* (pp. 32-60). Salt Lake City, UT: University of Utah Press.

Yataco Capcha, J. J., & Nami, H. G. (2016). A Reevaluation of Paleo American Artifacts from Jaywamachay Rockshelter, Ayacucho Valley, Peru. *PaleoAmerica, 2,* 368-372. https://doi.org/10.1080/20555563.2016.1199198

Ziólkowski, M. S., Pazdur Mieczyslaw, F., Krzanowski, A., & Michczynski, A. (1994). *Andes: Radiocarbon Database for Bolivia, Ecuador, and Peru*. Warsaw: Andean Archaeological Mission of the Institute for Archaeology, Warsaw University; Gliwice: Gliwice Radiocarbon Laboratory, Institute of Physics, Silesian Technical University.

Archaeological Discovery, 2021, 9, 113-134
https://www.scirp.org/journal/ad
ISSN Online: 2331-1967
ISSN Print: 2331-1959

The German Radar Station *La* 318 *Frosch*

Giancarlo T. Tomezzoli[1], Jean-Luc Moser[2]

[1]Etno-Archaeological Observatory, Munich, Germany
[2]Archives Municipales, Saint Malo, France
Email: gt21949@gmx.de, jean-luc.moser@sfr.fr

How to cite this paper: Tomezzoli, G. T., & Moser, J.-L. (2021). The German Radar Station *La* 318 *Frosch*. *Archaeological Discovery, 9,* 113-134.
https://doi.org/10.4236/ad.2021.92006

Received: February 25, 2021
Accepted: April 10, 2021
Published: April 13, 2021

Abstract

It is common opinion that WWII was characterised by small and great air, land and sea battles. This is true, but it ignores the role played by installations of advanced technology for collecting information about the enemy intentions. The German support point *La* 318 *Frosch* (*Frog*) at Cap Fréhel (Plévenon) near Saint Malo (Brittany—FR) is one of the best examples. Built among precedent military and civilian French signal components, it hosted sophisticated surveillance components. The visits conducted on the site, permitted to identify *La* 318 components, to determine their preservation state at about eighty years from the end of the WWII and to proceed to the components reconstruction.

Keywords

WWII, *La* 318, *Frosch*, *Goldfisch*, Radar, *Freya*, *Würzburg Riese*, *Mammut*, Cap Fréhel, Plévenon, Brittany

1. Introduction

It is common opinion that WWII was characterised by small and great air, land and sea battles. This is true, but it ignores the role played by installations of advanced technology for collecting information about the enemy intentions (Jones, 2009). The German support point (Stp—*Stützpunkt*) *La* 318 (Lamballe 318) *Frosch* (*Frog*) at Cap Fréhel (Plévenon) near Saint Malo (Brittany—FR) is one of the best examples. Built among precedent military and civilian French signal components, it hosted sophisticated surveillance components.

2. History

After precedent lighthouses, on 1702 on Cap Fréhel a headlight began its service burning at the beginning coal and after whale and rapeseed oil. On 1st May 1847 a new 1st class lighthouse began its service. Its two white pulses every 10 sec. were

visible up to 40 km. It had an octagonal tower 22 m high, 3.40 m in diameter with dependencies for guardian lodgments on the sides. On 1860, the municipality of Plévenon purchased for 60 Francs a 50 ares parcel (half hectare) from the French Navy for constructing an electro-semaphore in connection with that of Saint-Cast-Le-Guildo, on the place of an ancient telegraph. The electro-semaphore, T shaped, with large windows and no floors, was burned on 1940 by French soldiers before the arrival of German troops. From 1940, due to the German military interest, *La* 318 was developed, comprising surveillance and defensive components, under the direction of the *Oberbauleitung* Saint-Malo. A Decauville rail track was arranged for the transport of construction materials on the site (GLAD, 2020).

The sources are not in agreement about the surveillance radar in service at *La* 318, either: 1 × *FuMG* 401 *LZ Freya*, 1 × *FuMG* 65 *L Würzburg Riese* at *Stp I*; 1 × *Mammut* at *Stp II*; 1 × *FuMG* 450 *Flamme*, 1 × *FuMG* 65 *L Würzburg Riese*, 1 × *Würzburg* 39(*t*) at *Stp III* (Kerhousse, 2016); or: 1 × *FuMO* 214 *Würzburg Riese*, 1 × *FuMO* 2 *Calais B*; 2 × *FuMG* 65 *L Würzburg Riese*, 1 × *FuMG* 80 *Freya A/N* and later 1 × *FuMG* 401 *LZ Freya*, 1 × *FuMG* 80 *Freya* with *Gemse* and *A/N*, and still later 1 × *FuMG* 450 *Freya*, 1 × *FuSE* 62 *D*; 1 × *FuMG* 41 *G* (*cF*) *Mammut*, 1 × *FuMO* 214 (DAWA, 2016). A radar *FuMO* 2 was placed on top of the headlight for air and sea surveillance (DAWA, 2016; Powelei, 2012)—Appendix A1. A radio station was located in the lighthouse and five mine fields with stakes against glider planes were established.

In service took turn the 22./*LgNaRgt Westfrankreich*, 1. and 3. *FuMAbt*, 24./*LgNaRgt* 12 and after 5./*FlugmeldeLeitKp II./LnRgt* 54, 1/3 *FuMAbt Brest*. In total, *La* 318 garrison reached 230 officers and soldiers.

On 11th August 1944 the garrison destroyed the lighthouse, and, under the orders of lieutenant Sasse, on 30th August 1944 surrendered unconditionally to the American troops.

On 1945 the headlight restarted its service with a high tension provisional light and an emergency generator. On 1st July 1950 a new lighthouse began its service with a halogen lamp whose two white pulses every 10 sec. were visible up to 200 m in foggy and 110 km in clear weather. On 1952, the Touring-Club-de-France (founded in 1890) rented part of the Roche Jaune for facilitating the reception of tourists and prepared a platform, at the site of an ancient steam foghorn. On the platform, stands up the tower of a modern two sounds per minute foghorn (GLAD, 2020).

3. The Visits

The visits to *La* 318 (**Figure 1**) took place on 18 August 2005, 11 January 2011, 08 August 2020 and permitted to identify *Stp I*, *Stp II* and *Stp III* components (Kerhousse, 2016).

3.1. *Stp I*

The *Stp I* identified components (**Figures 2-8**) were the following.

A ditch (48˚40'49.64"N, 2˚19'27.94"W, height 57.74 m) (1), 45 x 16 m, about 713 m^2, provided with a side access ladder. On its floor, partially invaded by vegetation, two parallel concrete rails, spaced apart of 3.5 m. On the side walls, pebbles of the EroVili (Tomezzoli & Marzin, 2015) and formwork

Figure 1. *La* 318—*Stp I*; *Stp II*; *Stp III*; a Pointe du Jas; b Amas du Cap; c Roche Jaune; d lighthouse square; e nowadays parking; f Pointe du Château-Renard; g Lalande de Fréhel, h Cap Fréhel access road. [Geoportail]

element traces were visible. Its concrete structure, disfigured by a recent graffiti on the north side wall, was in good preservation state without damages due to combats.

A small bunker (48˚40'48.97"N, 2˚19'27.29"W, h 62.51 m) sunk into the terrain, 12 m south from the *L* 486. Its coverage was partially invaded by vegetation. A short access trench led to its entrance, which obstructed by vegetation, let the interior inaccessible. Its concrete structure was in a good preservation state without damages due to combats.

A water tank (*WBH* Wasserbehalter) bunker (48˚40'49.49"N, 2˚19'24.41"W, h 69.82 m) (2) (Powelei, 2012). Its entrance, invaded by vegetation, introduced into a 7.5 m long corridor, which preserved on its walls and ceiling the original white painting disfigured by modern graffiti and formwork element traces. At 90˚ left on the corridor end the entrance to an 6.5 × 3.5 m room. It preserved on its walls and vaulted ceiling the original white painting disfigured by modern graffiti and formwork element traces. On its back wall a 1.5 × 0.8 m, 50 cm

deep niche probably for room ventilation. The corridor and room concrete structure was in good preservation state without damages due to combats.

Figure 2. *La* 318—*Stp. I*: 1 ditch; 2 *WBH* bunker; 3 stone and brick construction; 4 *V* 229; 5-7 *Flak* emplacements; 8 *R* 622; 9 stone barrack; 10 *L* 479 *Anton* bunker. [Geoportail].

A construction (48˚40'49.64"N, 2˚19'23.61"W, h 71.24 m) (3) similar to a Middle.

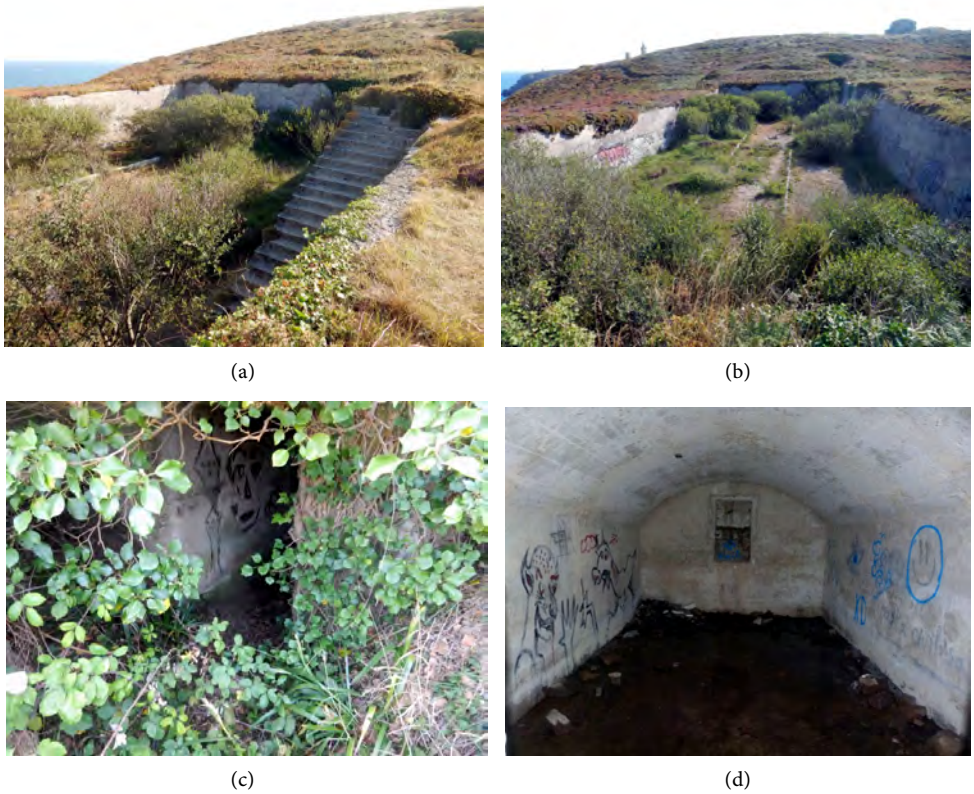

(a) (b)

(c) (d)

Figure 3. (a) ditch (1) access ladder; (b) ditch floor with concrete rails; (c) *WBH* bunker (2) entrance invaded by vegetation; (d) *WBH* bunker internal room.

(a) (b)

Figure 4. Stone and brick construction (3): (a) lower wing; (b) construction interior.

Ages one for *Freya* radar (Powelei, 2012)—Appendix A5. Around a 5 m high, 5 m in diam. cylindrical tower, a semi-circular wing of the same high toward east and a lower wing toward west. The *Freya* antenna was placed on the tower coverage, the instrumentation and personnel lodged at the interior. Its internal and external stone and brick structure, partially invaded by vegetation, was in good preservation state without damages due to combats.

A *V* 229 support (48˚40'51.6"N, 2˚18'32.75"W, h 65.09 m) (4) for radar *Würzburg Riese*—Appendix 5. A short metallic plate on the upper side protected its access opening on one of its side walls. The internal floor was covered by stones. On the internal walls two recesses for shelves or equipment were visible. On the upper side metallic fixation points and traces of the corresponding *Würzburg Riese* supporting elements were visible. On the walls, pebbles of the EroVili mixed with concrete were visible. The concrete structure was in good preservation state without damages due to combats.

A first RS 58c Tobruck (48˚40'48.81"N, 2˚19'31.4"W, h 63.43 m) with access trench and a second *RS* 58*c Tobruck* (48˚40'52.51"N, 2˚19'31.51"W, h 62.52 m) with access trench were visible although partially invaded by vegetation.

A 2 × 1.5 m open cistern (48˚40'49.78"N, 2˚19'32.23"W, h 64.17 m) similar to those observed at *Be*-2 at Mont Saint Michel de Braspart (Tomezzoli & Dupont,

(a) (b)

Figure 5. *V* 229 (4): (a) support for *Würzburg Riese*; (b) interior walls with two recesses for shelves or equipment.

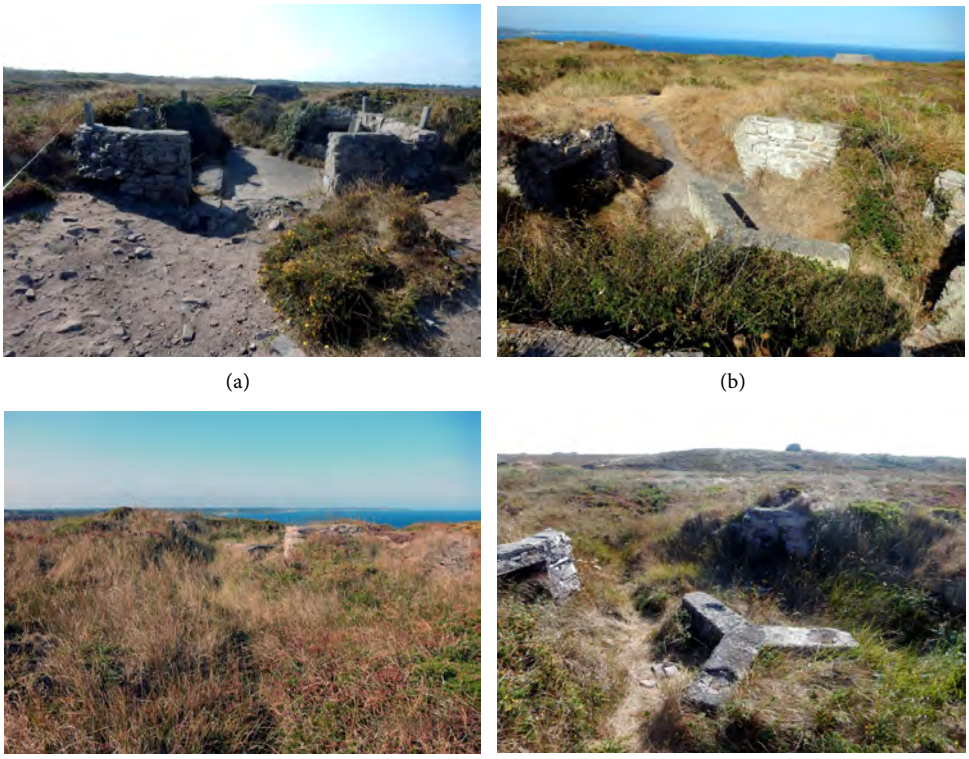

(a) (b)

(c) (d)

Figure 6. (a) first *Flak* emplacement (5); (b) second *Flak* emplacement (6) with Y gun support; (c) third *Flak* emplacement (7); (d) third *Flak* emplacement (7) with Y gun support.

2011). Its concrete structure was in a good preservation state without damages due to combats.

A first, rough in construction, octagonal *Flak* emplacement (48˚40'52.2"N, 2˚19'33.18"W, h 65.05 m) (5) manufactured by stones bound with concrete, without underground bunker. Three niches for ammunitions were visible on three corresponding side walls. On the floor, no Y support for gun holder legs. Its structure, partially invaded by vegetation, was in a good preservation state without visible damages due to combats.

A second, rough in construction, octagonal *Flak* emplacement (48˚40'52.37"N, 2˚19'32.52"W, h 63.98 m) (6) manufactured by stones bound with concrete, without underground bunker. Two niches for ammunitions were visible on two corresponding side walls. On the floor, a Y support for gun holder legs. Its structure, partially invaded by vegetation, was in a good preservation state without visible damages due to combats.

A third, rough in construction, octagonal *Flak* emplacement (48˚40'50.66"N, 2˚19'32.99"W, h 65.37 m) (7) manufactured by stones bound with concrete, without underground bunker. One niche for ammunitions was visible on one side wall. On the floor, a Y support for gun holder legs, with a circular niche on each Y arm. Its structure, partially invaded by vegetation, was in a good preservation state without visible damages due to combats.

A *R* 622 bunker (48˚40’51.15”N, 2˚19’31.04”W, h 64.94 m) (8) for two groups

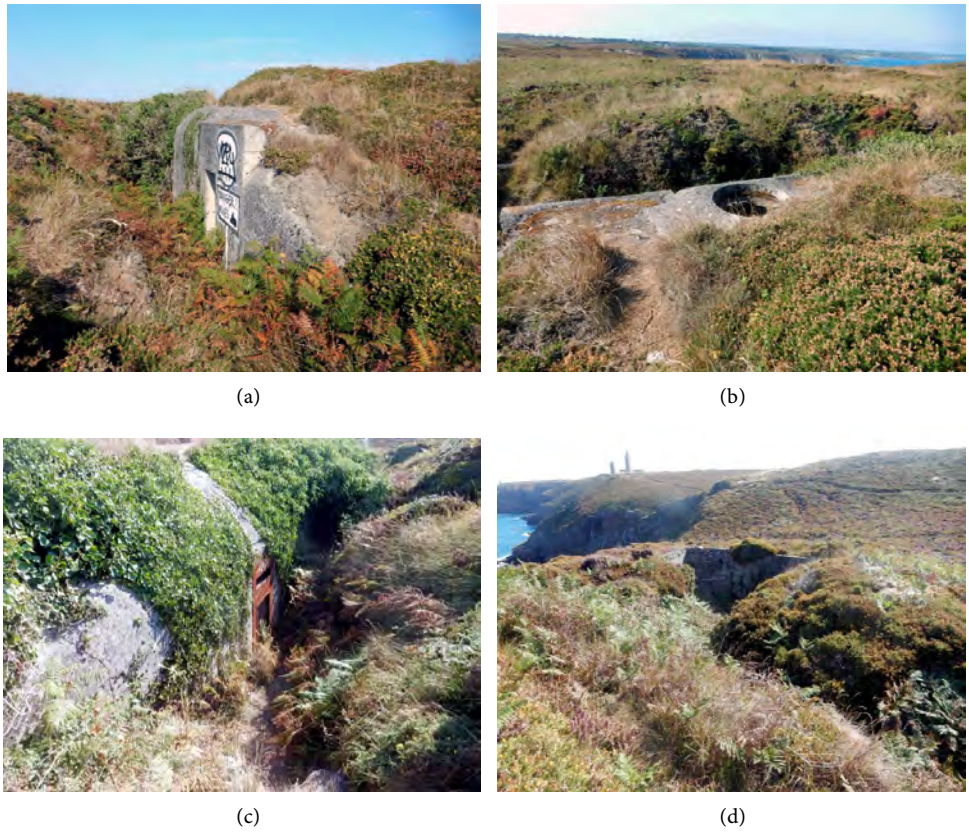

(a) (b)

(c) (d)

Figure 7. (a) *R* 622 (8) entrance of the observation post; (b) *R* 622 observation post aperture; (c) *R* 622 entrance; (d) stone barrack or water reservoir (9).

each of ten soldiers (Rudi, 1988), partially covered by vegetation. On the coverage, the circular aperture of the observation post with a circular metal ring and three circular concrete emplacements each with a 10 cm in diam. circular aperture. Two entrances were obstructed by vegetation and recent barriers, so that the interior remained inaccessible. However, one of said entrances let visible a descending ladder with original white and orange wall paintings and rusted ceiling metal portions. The concrete structure was in good preservation state without visible damages due to combats.

A 3 × 5 m stone barrack or water reservoir (48˚40'51.25"N, 2˚19'30.26"W, h 62.08 m) (9). The floor was invaded by stones and vegetation and its access trench was still visible on the terrain. The stone structure was severely degraded.

An *L* 479 *Anton* bunker (48˚40'47.07"N, 2˚19'22.73"W, h 69.78 m) (10) for night-fighter control (Fleuridas et al., 2010)—Appendix A2-A3, similar respectively to that of the radar camp at Saint-Pabu-Le Bous (Tomezzoli & Colliou, 2017a; Tomezzoli & Colliou, 2018) and at Saint-Jacques de la Lande near Rennes (Dupont et al., 2007). Pebbles of the EroVili and traces of formwork elements were visible on the façade. The entrances were obstructed by recent barriers and vegetation, so that the interior remained inaccessible. However, the re-cooling room conduit let visible the original white wall painting. Its concrete structure, disfigured by recent graffiti, was in good preservation state without damages due

(a) (b)

(c) (d) (e)

Figure 8. *L* 479 bunker (10): (a) observation post entrance; (b) facade; (c) observation post interior; (d) façade detail; (e) re-cooling room conduit with original white painting.

to combats.

3.2. *Stp II*

The *Stp II* identified components (**Figures 9-12**) were the following.

An *L* 485 bunker for radar *FuMG* 41 *G* (*cF*) *Mammut Caesar* (48˚40'33.34"N, 2˚19'14.6"W, h 74.38 m) (1) (DAWA, 2016) invaded by vegetation—Appendix A4. The façade let visible pebbles of the EroVili and formwork element traces. Although disfigured by modern graffiti, it was in good preservation state without damages due to combats. Two rectangular pylons protruding from the coverage and invaded by orange lichens at the top were in good preservation state. A cylindrical tube emerged from the top of the west one. An entrance gave access to an observation post surprisingly clean, without internal walls painting. Another entrance, preserving its original white painting and defense loophole at the ladder end, allowed access to the interior. The internal rooms were surprisingly clean and in good preservation state without damages due to combats. The walls preserved their original white and orange paintings here and there disfigured by modern graffities and formwork element traces. On the floors the original tiling was still in place and the ceilings appeared severely rusted. The compensator room preserved on one wall the main entrance for instrumentation and

Figure 9. *La* 318—*Stp II*: 1 bunker *L* 485 for radar *FuMG* 41*G* (*cF*) *Mammut Caesar;* 2 barrack; 3 possible *RS* 58*c Tobruck*, 4 water reservoir/pool; 5 *Flak* emplacement; 6 *Flak* emplacement. [Geoportail].

(a) (b)

(c) (d)

Figure 10. *L* 485 (1): (a) protruding rectangular pylons; (b) observation post entrance; (c) façade with modern graffities; (d) entrance with defense loophole.

(a) (b)

Figure 11. *L* 485: (a) internal room, on the right wall defence loophole on the left wall metallic support of unknown purpose; (b) compensator room.

materials obstructed by terrain and on each adjacent side wall the access to the antenna room. Each access had 12 circular cable passages on each side. On the floor a 3 × 2 m rectangular support for the compensator, with two square supports on each longer side. Another 1 × 0.5 m rectangular support with a fixation point at each angle was aligned with the shorter side. The antenna room ceiling had twenty four cable accesses toward the corresponding external protruding pylon. All the technical instrumentations and furniture disappeared.

A 15 × 13 m barrack (48˚40'34.22"N, 2˚19'12.07"W, h 67.08 m) (2). The roof disappeared and because of vegetation coverage, the interior remained inaccessible. The stone structure was severely degraded.

A possible *RS* 58*c Tobruck* (48˚40'32.91"N, 2˚19'11.32"W, h 66.77 m) partially invaded by vegetation.

A 6 × 10 m barracks (48˚40'32.7"N, 2˚19'11.36"W, h 69.06 m) near the *RS* 58*c*. Because of vegetation coverage, the interior remained inaccessible. The stone structure was severely degraded.

(a) (b)

Figure 12. *L* 485: (a) gas lock and antenna room; (b) antenna room ceiling.

A 7 × 10 m, 1.5 m deep water reservoir/pool (48˚40'35.19"N, 2˚19'16.35"W, h 71.31 m) (4). Completely invaded by vegetation, it remained inaccessible.

A first 2.5 × 2.0 m *Flak* emplacement (48˚40'35.52"N, 2˚19'16.84"W, h 73.04

m) (5) with a 3 m long access passage. Completely invaded by vegetation, it remained inaccessible.

A second 2.5 × 2.0 m *Flak* emplacement (48˚40'33.51"N, 2˚19'15.54"W, h 74.35 m) (6) without access passage. Completely invaded by vegetation, it remained inaccessible.

A third 2.5 × 2.0 m *Flak* emplacement (Powelei, 2012). Completely invaded by vegetation its position identification was not possible.

3.3. *Stp III*

The *Stp III* identified components (**Figures 13-18**) were the following.

A *V*229 support (48˚40'55.95"N, 2˚18'0.3"W, h 66.4 m) (1) for radar *Würzburg Riese*. The interior invaded by vegetation was not accessible. On the upper side the metallic fixation points and the traces of the corresponding *Würzburg Riese* supporting elements were visible. On the walls, pebbles of the Ero Vili mixed with concrete were visible. The concrete structure was in good preservation state without damages due to combats.

A 4 × 6 m SEA power generator aggregate (*Stromerzeuger aggregat*) bunker (48˚40'55.95"N, 2˚19'0.3"W, h. 67.04 m) (2) (Lippmann, 2018) invaded by vegetation, the entrance closed by a wood barrier remained inaccessible. The coverage was 1 m thick and on the entrance side 7 vertical camouflages slits were visible. The concrete structure was in good preservation state without damages due to combats.

A 4 × 5 m bunker (48˚40'56.44"N, 2˚19'5.21"W, h. 68.9 m) (3) buried in the terrain. The concrete coverage was in good preservation state without damages

Figure 13. *La* 318 *Stp III*—1 *V*229; 2 small bunker; 3 buried bunker; 4 rectangular structure; 5-7 circular areas; a nowadays parking; b Cap Fréhel lighthouse access road [Geoportail].

(a) (b)

Figure 14. *VF* 229: (a) support for *Würzburg Riese*; (b) imprint of the radar connection.

due to combats.

A 17 × 6 m structure (48˚40'56.27"N, 2˚19'5.82"W, h. 70.29 m) (4), S/W-N/E oriented, of rectangular shape with rounded short sides, invaded by vegetation. The N/E side hosted the entrance, the interior four aligned circular gun emplacements, the S/W side disappeared under the Cap Fréhel lighthouses access road (b).

A *FuMo* 2 *Seetakt* emplacement near the lighthouse of 1950 remained unidentified.

A first 30 m in diam. circular area (48˚40'49.37"N, 2˚19'8.28"W, h. 69.39 m) (5), a second 10 m in diam. circular area, (48˚40'47.55"N, 2˚19'9.46"W, h. 63.56 m) (6) and a third 35 m in diam. (48˚40'49.18"N, 2˚19'10.17"W, h. 63.34 m) (7) located about 200 meters S/W of the nowadays parking (48˚40'54.05"N, 2˚19'3.3"W, h. 66.67 m) (a). They were evident because of different colour and height of their moorland grass with respect to that of the surroundings.

Two storage bunkers, two cisterns, a stone personnel bunker with concrete coverage, a bunker with *Flak* open emplacement (OBFla), a *VF* 229, a *VF* machine bunker (*Trafostation*), two tobruck, an ammunition bunker, a *Freya FuSE* 80 emplacement, two *Flak* emplacements (Powelei, 2012) about 130 m south of the a nowadays parking (a), invaded by vegetation, remained inaccessible.

The French Batterie Est (48˚41'13.87"N, 2˚19'1.36"W, h. 61.09 m) and Batterie

(a) (b)

Figure 15. (a) small bunker (2); (b) lighthouses square, on the left the headlight, on the right the 1950 lighthouse with dependencies.

(a) (b)

(c) (d)

Figure 16. (a) 30 m in diam. circular surface; (b) 10 m in diam. circular surface; (c) 32 m in diam. circular surface; (d) a room of the French ammunition depot.

Ouest (48˚41'13.79"N, 2˚19'3.37"W, h. 58.33 m), on Roche Jaune, each comprising a platform with two in barbette parallel 95 mm Lahitolle 1888 or 1914/18 gun emplacements each formed by a concrete arc connected by three concrete segments to a central, circular six bolts metallic support, observed during the 11 January 2011 visit, disappeared.

A nearby circular concrete gun emplacement (48˚41'15.2"N, 2˚19'3.12"W, h. 58.87 m) with 14 circularly disposed fixation bolts for 9.5 cm French Canon de Côte 95 M93, identified during the 11 January 2011 visit, disappeared.

(a) (b)

Figure 17. Roche Jaune: (a) semaphore emplacement, on the background the foghorn tower, (b) semaphore emplacement circular surface, on the background lighthouse and headlight.

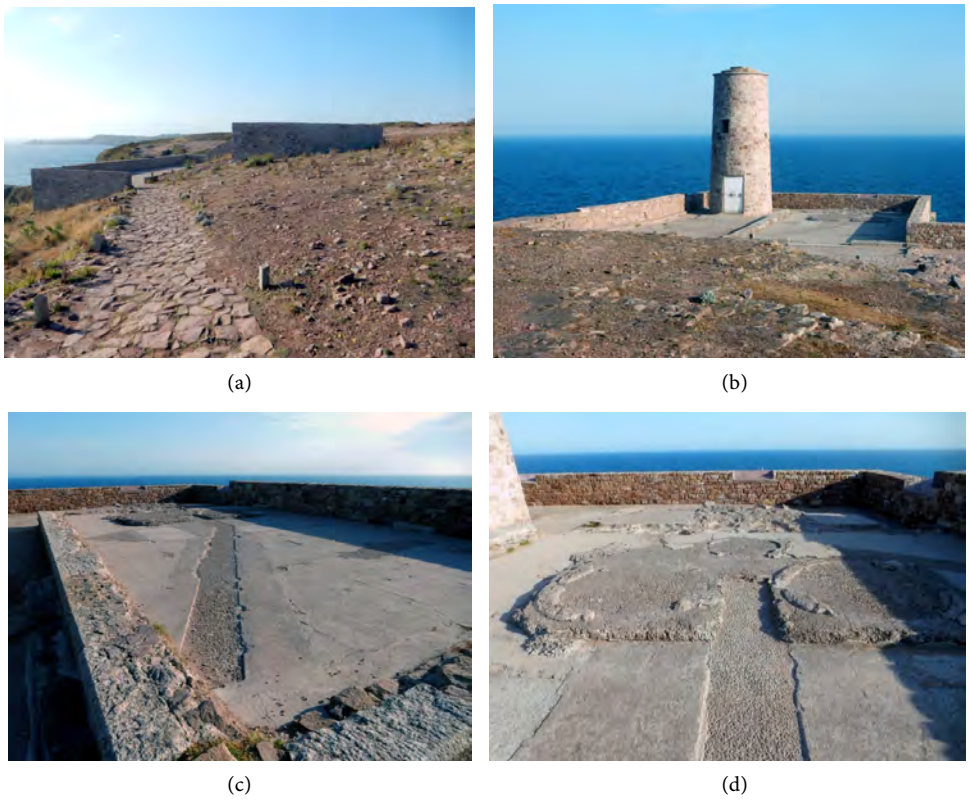

(a) (b)

(c) (d)

Figure 18. Roche Jaune: (a) belvedere; (b) foghorn platform, on one side the nowadays foghorn tower, on the other side emplacement of the old foghorn house, (c) old foghorn house, rests of the perimeter walls and diagonal covered trench; (d) old foghorn house, structures on the floor.

The 6 × 8 m semaphore emplacement (48˚41'13.5"N, 2˚19'2.01"W, h. 62.19 m). The two houses forming its T shape disappeared. The perimeter walls disappeared and on the concrete floor a 2.5 m in diam. circular surface was visible.

A belvedere (48˚41'7.91"N, 2˚18'59.34"W, h. 57.23 m) with stone walls formed by a 6 × 21 m rectangular platform and a 2 m higher 14 m in diam. semi-circular platform. It resulted from the 2012 demolition of the restaurant La Fauconnière built on the 1920s and present at *La* 318 during the WWII.

Three rings on the terrain for anchoring a disappeared French semaphore mast, observed during the 18 August 2005 visit, disappeared.

The 13 × 13 m foghorn platform (48˚41'16.09"N, 2˚19'3.21"W, h. 56.83 m). On one side the tower of the nowadays foghorn in good preservation state, on the other side the 7 × 10 m concrete emplacement of the old foghorn house. Rests of house perimeter walls were visible. On the concrete floor a diagonal, concrete covered trench for electrical cables, connected to three in triangular disposition 1 m in diam. concrete, circular emplacements. They formed the bases of the foghorn vapour generators. In front of the circular emplacements the semi-circular coverage rests of the of the water cisterna.

4. Discussion

The majority of the literature sources identify the *La* 318 (Rapport Pinczon du

Sel, 1947-1948) cover name as *Frosch*, except two (Glad, 2020; Lippmann, 2018) which identify the cover name as *Goldfish*. However, the radar station *Goldfish* was at Guernsey, one of the Channel Islands (DAWA, 2016). Therefore, the identification of these two sources is incorrect.

Substantially, *La* 318 repeats the architecture of *Stp Re* 510 (Renan 510) *Pinguin* at Saint-Pabu-Le Bous (Tomezzoli & Colliou, 2017a) near Brest, of *Funkmeßstellung* 2. *Ordnung Mandrill* at Monterfil (Dupont et al., 2007; Tomezzoli & Pottier, 2015) near Rennes and *Funkmeßstellung* 1. *Ordnung Made* at Les Mées (Dupont et al., 2007) near Le Mans essentially based on two *Freya* and two *FUSE* 65 *Würzburg Riese*. Two *Freya* and two *Würzburg Riese* were necessary for assuring continue surveillance also in case of maintenance or malfunctioning of one of them.

Mammut Caesar was an early warning radar able to detect aircrafts up to 300 km in two directions perpendicular to its rectangular antenna, but blind in a range of 60˚ on the antenna sides. *Freya* was an early warning radar detecting aircrafts up to 200 km but unable to determine their altitude. *Würzburg Riese*, often coupled to an IFF (Identification Friend Foe) device, was a near field warning radar detecting aircrafts up to 70 km, their azimuth and their altitude. Therefore, incoming aircrafts were first intercepted by the *Mammut* and *Freya* and after by the *Würzburg Riese* which, in case of foe aircrafts, provided data for directing the fire of the *Flak* emplacements. During day and night aircraft interceptions, the personnel of *L* 479 *Anton* collected all the available radar information and drove at least two interceptors against the target aircraft/s. The second interceptor was directed on the target aircraft/s in case of failure of the first one (Trenkle, 1979).

The personnel in service at *La* 318 lodged mainly in the lighthouse dependencies and in wood barracks on the right side of the lighthouses access road (b) (h). However, no barrack rests were identified.

4.1. *Stp I*

The presence of the *L* 479 *Anton* indicates that the *Stp I* components pertained to the *Luftwaffe*, as in the case of Saint-Pabu-Le Bous (Tomezzoli & Colliou, 2017a).

The ditch reminds the barrack emplacements (6)-(10) observed at the *Stp* Menez-Hom (Tomezzoli, 2017b). It protected either a large barrack or barracks (Lippmann, 2018; Powelei, 2012) or electrical generators (GLAD, 2020). The sources would not be in contradiction if the electrical generators were lodged in the large barrack or barracks, today disappeared, laid on the observed concrete rails. However, it is also possible that said large barrack or barracks lodged personnel. The ditch was covered with camouflage nets.

A 22 x 16 m rectangular excavation (48˚40'48.26"N, 2˚19'24.16"W, h. 64.51 m) between *L* 486 and *L* 489, identified in a French air reconnaissance image (C3639-0531_1948_MISSIONBRETAGNE16AV, n˚146, 1/26228, Argentique, 14/05/1948) escaped identification because the vegetation coverage.

A *R* 656 for fifteen soldiers has been signalled (Lippmann, 2021), but its presence has not been identified.

Candidates for the *Flak* emplacements were either a 2 cm single Flak 30, or a 2 cm *Flakvierling* 38 or a 3.7 cm Flak 18/36/37 gun.

4.2. *Stp II*

The presence of the *FuMG* 41 *G* (*cF*) *Mammut Caesar* indicates that the *Stp II* components pertained to the *Luftwaffe.*

Because no personnel lodgement was foreseen inside the *L* 485 the personnel lodged in the two nearby barracks. It is possible that either the smaller one hosted a kitchen/canteen and the bigger one personnel lodgements. The disappeared technical instrumentations and furniture were probably confiscated by the American or French army.

The absence of the radar antenna in said 1948 French air reconnaissance image indicates that it was dismantled before 14/05/1948. Actually, antenna portions were used for the construction of cereals silos in a nearby farm.

The water reservoir/pool, already observed at the Murs-Erigné German base (Tomezzoli, 2016) and the Domaine de Pignerolle (Tomezzoli et al., 2013) provided relax to the personnel and water in case of fire in the *Stp II* components.

Candidates for the *Flak* emplacements were either a 2 cm single Flak 30, or a 2 cm *Flakvierling* 38 or a 3.7 cm Flak 18/36/37 gun.

4.3. *Stp III*

The *Stp III* components pertained to the *Kriegsmarine*, as in the case of Saint-Pabu-Le Bous (Tomezzoli & Colliou, 2017a).

The rectangular structure (4) was a four guns in barbette French battery, preceding *La* 318. Because of its open structure, the guns might defend the whole Cap Fréhel.

The three circular surfaces (5)-(7) were probably whip antenna emplacements. This is suggested by the radio station was located in the lighthouse (GLAD, 2020) and a corresponding reinforced field-like *Vf* (*Verstärkt feldmässige*) telecommunication (*Fernmelde stand*) bunker (Lippmann, 2018) which unfortunately was not identified and no concrete antenna cable fixing block was identified.

An east and west parallel 20 x 6 m barrack on the of the Cap Fréhel lighthouse square, visible in said French air reconnaissance image, hosting respectively the kitchen/canteen and officers lodgements (Glad, 2020) disappeared before 21/05/1952 (C3639-0531_1948_MISSIONBRETAGNE16AV, n˚146, 1/26228, Argentique, 14/05/1948; C1215-0101_1952_F0915-1215_0002, n˚2, 1/25842, Argentique, 21/05/1952).

The French Batterie Est and Batterie Ouest constituted a defence against ships and submarines. Especially these last, because of their limited autonomy and the danger of navigating in immersion near the coast often emerged and engaged the coastal defences by their gun.

5. Conclusion

This article permitted us to put order in a lot of information concerning *La* 318 and other precedent and coexisting French military and civilian structures on Cap Fréhel and to present the information in an organic way accessible to a public of experts and amateurs. We hope that this article will stimulate further studies on other WWII installations of advanced technology, because they influence on military operations, life and fate of thousands of men.

Acknowledgement

The authors are grateful to Mr Fleuridas P. for his explanations and his kind permission to insert in the Appendix the plants of the bunkers *L* 479 *Anton* and *L* 485.

Conflicts of Interest

The authors declare no conflicts of interest regarding the publication of this paper.

References

DAWA (Deutsches Atlantikwall-Archiv) (2016). *Deutsches Atlantikwall Archiv*. Stand: 17. Dezember 2016. http://www.atlantikwall.info

Dupont, Ph., Fresil, Y., & Tomezzoli, G. (2007). Deutsche Militärbauten bei Rennes. *DAWA Nachrichten, 49,* 56-66.

Fleuridas, P., Herbots, K., & Peeters, D. (2010). *Constructions Normalisées de l'Armée de l'Air*. *Regelbauten der Luftwaffe*. France: Ed. des Auteurs.

GLAD (2020). *L'Inventaire du Patrimoine Culturel de Bretagne*. http://patrimoine.bzh

Jones, R. V. (2009). *Most Secret War*. *British Scientific Intelligence 1939-1945*. London: Penguin Books.

Kerhousse, Y. (2016). *Côtes du Nord* 1940-1944. *Les installations radar allemandes. De la pointe du Cap Fréhel et leur environnement historique*. Plérin: Association GERFRAUT.

Lippmann, H. (2018). *La* 318 *Goldfisch—Map F3 2118 010B [F3 203]*.

Lippmann, H. (2021). *Private Communication*.

Powelei, J. (2012). *LA* 318 *Frosch. Cap Fréhel. Map 08/2012*.

Rapport Pinczon du Sel (1947-1948). *Le Mur de l'Atlantique la Cote de la Manche et de l'Atlantique du Mont Saint-Michel à Laita*. Service Historique de la Marine. Brest, Livre IV. Plan No. 23 IV.

Rudi, R. (1988). *Typologie du Mur de l'Atlantique*. NUGI 923. Amsterdam: Beetsterzwaag.

Tomezzoli, G. T. (2016). The German Base "The Bank" at Mûrs-Érigné (Anjou-FR). *Archaeological Discovery, 4,* 37-47. https://doi.org/10.4236/ad.2016.41004

Tomezzoli, G. T. (2017b). The WW II German *Stützpunkt* on the Menez-Hom (Finistère-FR). *Archaeological Discovery, 5,* 224-237. https://doi.org/10.4236/ad.2017.54013

Tomezzoli, G. T., & Colliou, S. (2017a). The WW II Saint-Pabu German Radar Camp and the *Stützpunkte Re* 03, *Re* 04. *Archaeological Discovery, 5,* 142-162.

https://doi.org/10.4236/ad.2017.53009

Tomezzoli, G. T., & Colliou, S. (2018). The WW II Saint-Pabu German Radar Camp-2. *Archaeological Discovery, 6,* 88-102. https://doi.org/10.4236/ad.2018.62006

Tomezzoli, G., & Dupont, Ph. (2011). Die Drehfunkfeueranlage Bernhard auf dem Mont Saint Michel de Brasparts. *DAWA Nachrichten, 57,* 4-15.

Tomezzoli, G., & Marzin, Y. (2015). The Ero Vili and the Atlantic Wall. *Advances in Anthropology, 5,* 183-204. https://doi.org/10.4236/aa.2015.54018

Tomezzoli, G., & Pottier, L. (2015). Die deutschen militärlogistischen Anlagen westlich von Mamers. *DAWA Nachrichten, 65,*14-27.

Tomezzoli, G., Pottier, L., Marquet, C., & Letertre, M.(2013). Les Installations de la Kriegsmarine au Domaine de Pignerolle. *39-45 Magazine,* 60-72.

Trenkle, F. (1979). *Die deutschen Funk-Navigations-und Funk-Fürungsverfahren bis* 1945. Stuttgart: Motorbuch Verlag.

Appendix

A1: reconstruction—*FuMO* 2 on top of the headlight for air and sea surveillance.

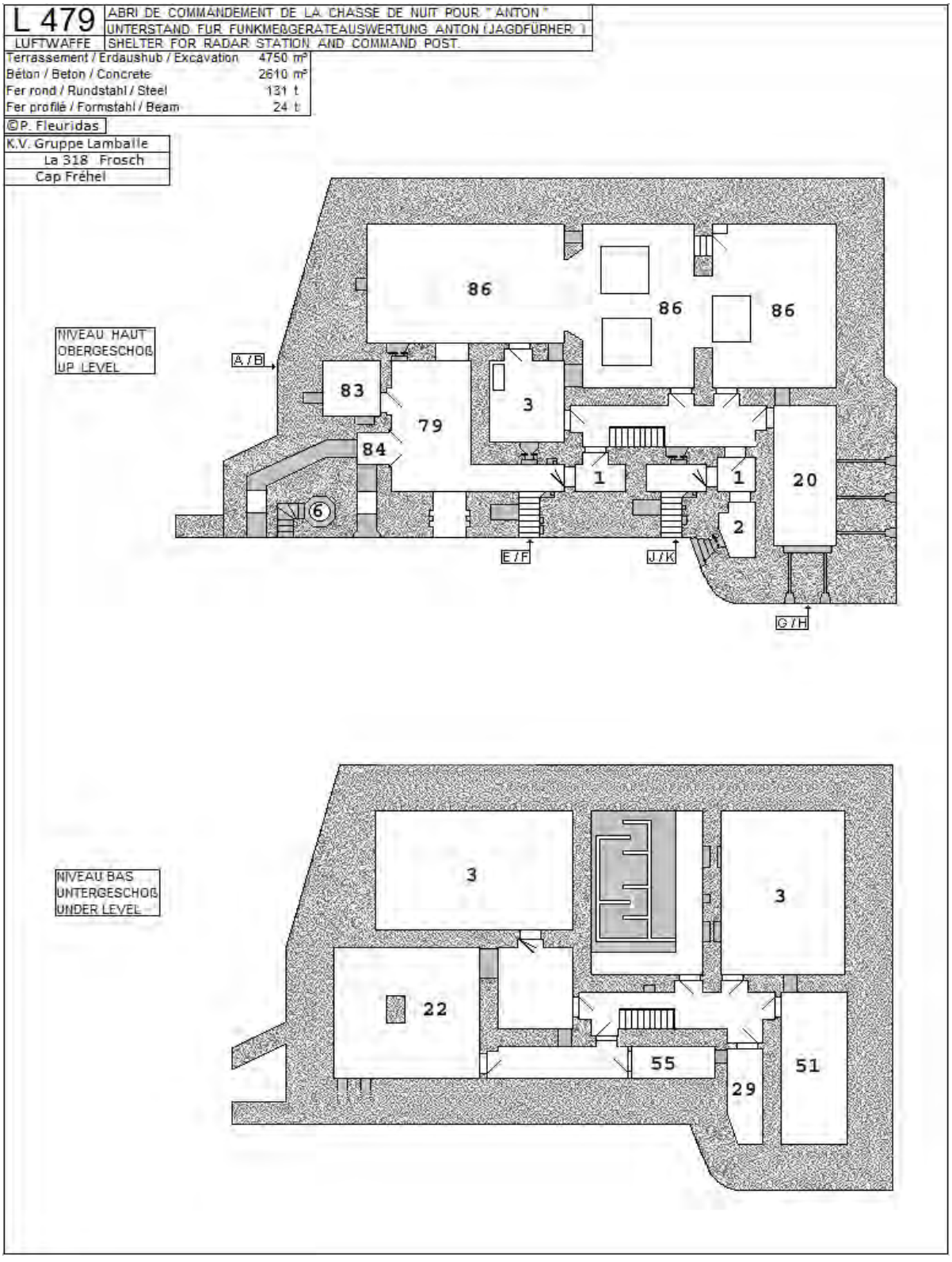

A2: *L* 479 *Anton* bunker for night-fighter control plan—1 gas lock, 2 close combat room, 3 crew room, 6 observation post, 20 wireless room, 22 ventilation room, 29 store room, 51 telephone exchange room, 55 store, 79 emergency generator room, 83 transformer room, 84 re-cooling room, 86 command post, 99 fuzes room (Courtesy Fleuridas P.) (Room numbering according to Rudi, 1988).

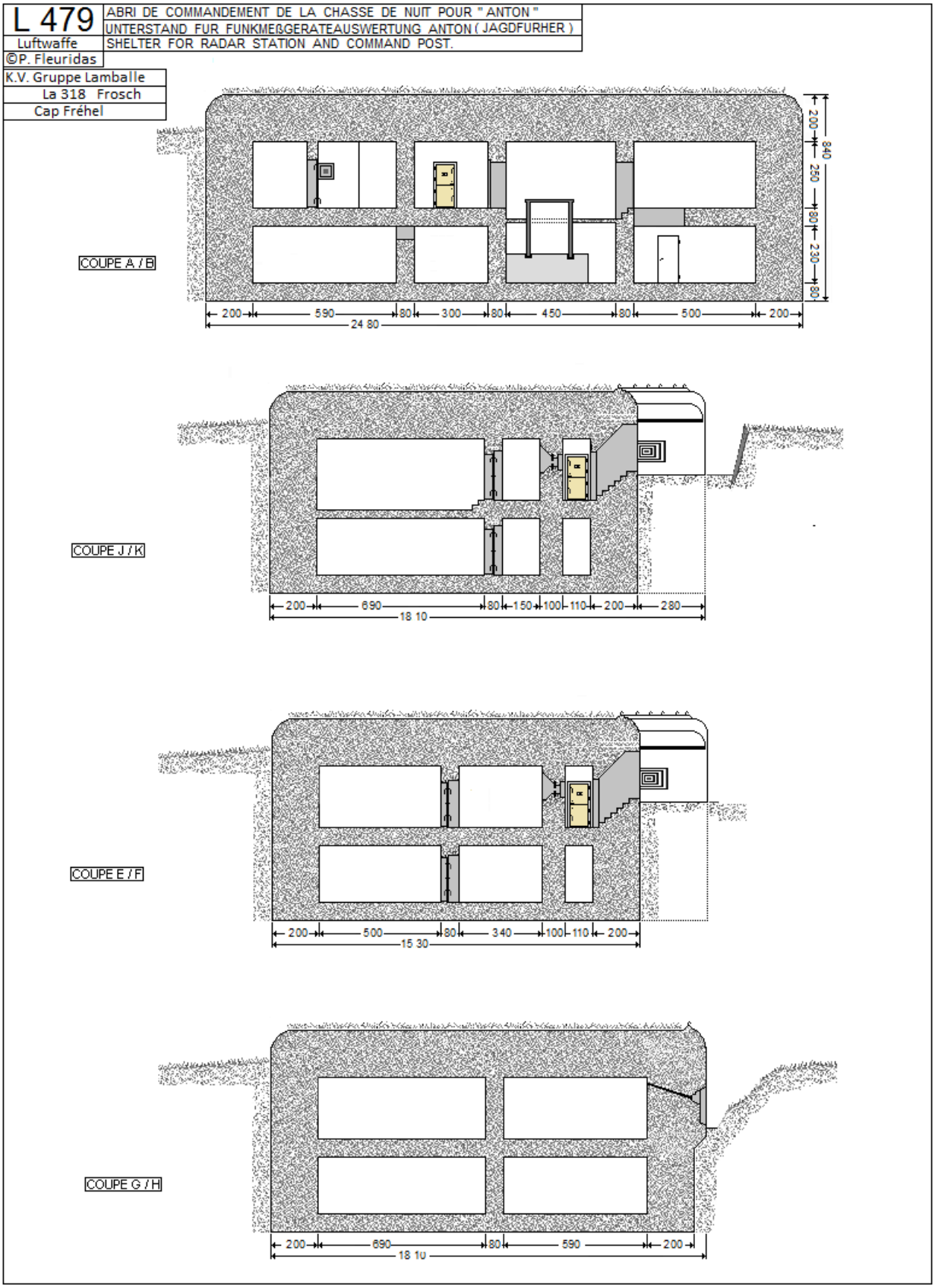

A3: *L* 479 *Anton* bunker for night-fighter control plan (Courtesy Fleuridas P.).

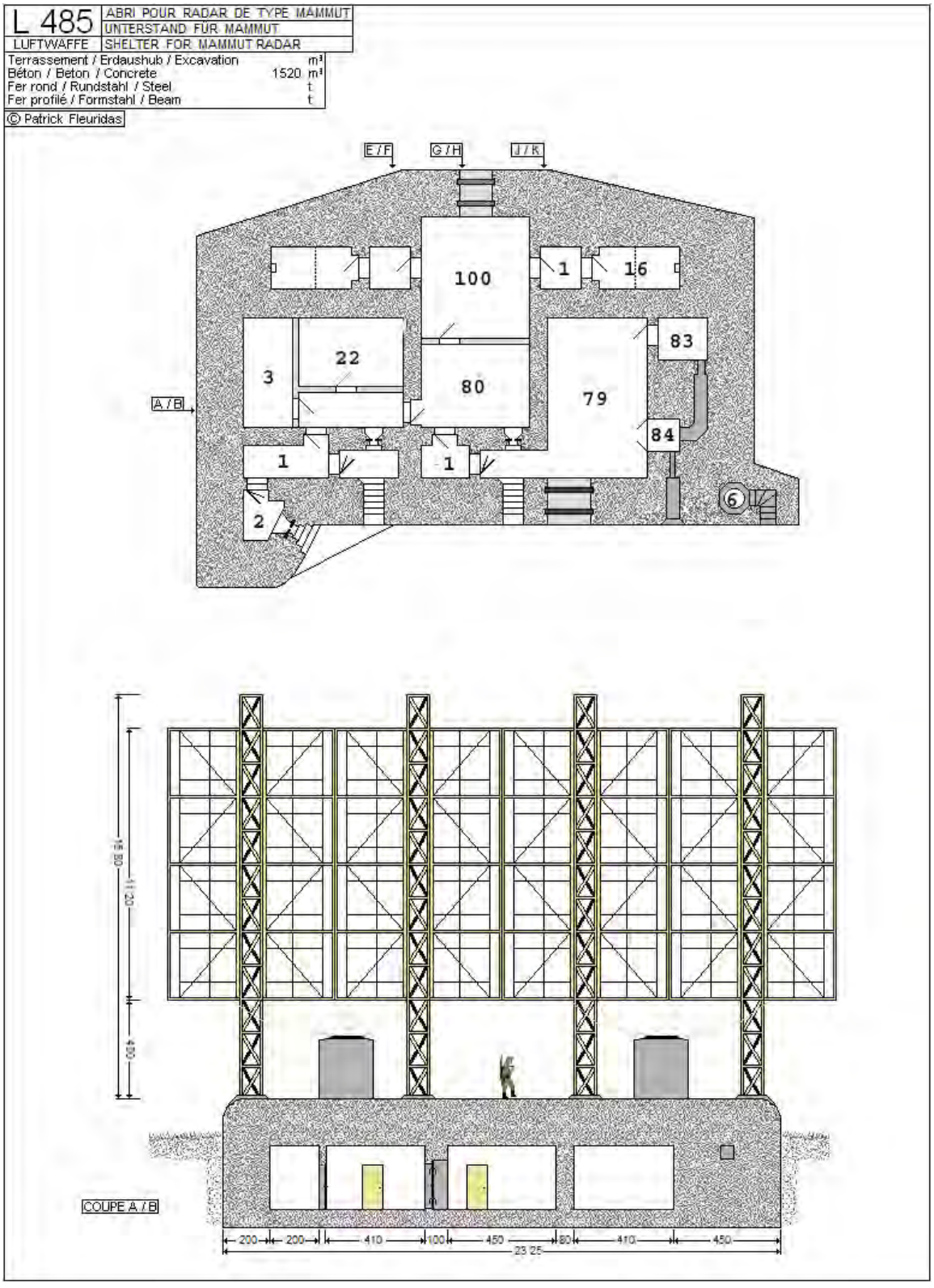

A4: bunker *L* 485 and radar *FuMG* 41*G* (*cF*) *Mammut Caesar*: 1 gas lock, 2 close combat room, 3 crew room, 6 observation post, 16 antenna room, 22 ventilation room, 79 emergency generator room, 80 workshop, 83 transformer room, 84 re-cooling room, 100 compensator room (Courtesy Fleuridas P.) (Room numbering according to Rudi, 1988).

A5: reconstruction—*FUSE* 65*L Würzburg Riese* on *V*229, in the foreground *FuMG*401 *Freya LZ* (radar image from a non-copyright site).

Archaeological Discovery, 2021, 9, 135-150
https://www.scirp.org/journal/ad
ISSN Online: 2331-1967
ISSN Print: 2331-1959

Evaluation of the Disparity Effect in the Amounts of Weathering Agents on the Archaeological Pine Wood "*Pinus sp.*"

Mahmoud Ali

Conservation Department, Faculty of Archaeology, Luxor University, Luxor, Egypt
Email: dr.mahmoud.sayed82@gmail.com

How to cite this paper: Ali, M. (2021). Evaluation of the Disparity Effect in the Amounts of Weathering Agents on the Archaeological Pine Wood "*Pinus sp.*". *Archaeological Discovery, 9,* 135-150.
https://doi.org/10.4236/ad.2021.92007

Received: March 9, 2021
Accepted: April 19, 2021
Published: April 22, 2021

Abstract

The aim of this research is to focus on the deterioration appearances of Pine wood "*Pinus sp.*" that has been widely used as an external architectural element in Egypt. The wooden lintels in this research were exposed to the influence of weathering factors which are varying in their amounts. This variation in the amounts was reflected in the appearance of the surface, at the anatomical structure of the pine wood, and at the changes in the main components of wood. To clarify all these changes, a comparison was made between wooden lintels exposed to two kinds of environments. Some very small samples from these environments had been chosen and examined by using the digital microscope and the Scanning Electron Microscope (SEM) which clarify the surface and anatomical changes of deteriorated wood. The Fourier transform Infrared Spectroscopy (FTIR) was used also to show the extent of changes in the main wood components. The results showed a clear difference in the surface, anatomical and chemical changes in the wood at these two different environments. In the first environment with high moisture levels, the wood was damaged more than in the other environment with high-temperature levels.

Keywords

Pine Wood, *Pinus sp.*, Lintels, Weathering, SEM, FTIR

1. Introduction

Wood is an essential material in archaeological and historical buildings. It was used as an architectural element and as a furniture in these buildings (Iruela, 2020). Wooden lintels, which consist of one or more pieces of wood placed above the doors and windows, are an example of these architectural elements,

especially in these buildings built with red and adobe bricks.

Pine wood "*Pinus sp.*" is one of the softwood types (Wiemann, 2010), it has been widely used as an architectural element in archaeological and historical buildings in Egypt. Although that the pine wood is one of the imported woods, we notice its wide spread in Egypt through different ages and in many purposes such as: ceilings, lintels, doors, windows, mashrabiyas and columns.

The aim of this research is to focus on deteriorated pine wood, which was used in making some lintels at the mausoleum of Fatma Khatun (1283-1284) (AH 682-683) wife of Sultan Qalawun. This mausoleum is situated at Al-Ashraf Street, Al-Khalifa district, Cairo, Egypt. This building needs necessary restoration works, not only for the wooden elements but for the entire building sunken in the groundwater (**Figure 1**).

The wooden lintels of this mausoleum are directly exposed to the surrounding weathering factors which are: moisture, temperature, sunlight, air pollutants, and wind. Also, the factor of abandonment and neglect exacerbated the deterioration aspects of the wooden elements such as the exposure of some window lintels in the outer portico to burn (**Figure 2**).

Figure 1. The wooden lintels at the mausoleum of Fatma Khatun.

Figure 2. (A)-(C), shows the burn of some window lintels in the outer portico of Fatma Khatun mausoleum, (C) SEM micrograph. 20 μm.

The literature review monitored many aspects of changes spread in softwood including the *Pinus sp.* exposed to weathering conditions. We concluded from these researches that we can divide these changes as follows.

Surface changes: as the roughness of the wood surface, resulting from the dispar-

ity in erosion rates of earlywood and latewood. The increasing of the earlywood erosion rate is associated with its low density (Oberhofnerová et al., 2017).

The weathered surface becomes infected with weakness and fragility, resulting from the loss of bonding between the wood fibers, which leads also to erosion and the loss of some parts from the surface (Feist, 1983; Feist, 1990). The alternation between exposure to sunlight and to the high levels of moisture leads to the spread of various cracks on the wood surface.

These cracks can sometimes lead to the split of wood, also they allow the weathering agents to penetrate to the internal parts of the wood. The cracks are considered as a suitable place for the activity of biological damage inside the archaeological wood (Teles & Valle, 2001). The chromatic change of wood surface is a significant change resulting from the exposure of wood to the weathering factors. A previous research noted that the surface of light wood turns to a dark color, on the other side, the surface of the dark wood turns to a light color in the early phases of weathered wood. This process is associated with lignin decomposition (Oberhofnerová et al., 2017).

Anatomical changes: In general, a significant weakness in the structure of wood can be noticed in the archaeological samples treated by the previous researches. It has been observed the spread of some checks and cracks in the cell wall layers, the separation of the cell wall layers, destruction of the bordered pits (Hamed et al., 2020), destruction and loss of the middle lamella which lead to the detachment of wood cells from each other, and to the breakdown of cells walls and its layers (Hamed, 2014).

Chemical changes: Weathering factors affect the chemical compounds of wood, in particular the surface of archaeological and historical wood exposed directly to the sunlight, affecting the strength, the durability of wood, and the cohesion of the surface, In addition to the color changes, which are considered as a remarkable sign of the wood deterioration (Sandberg, 1999). The photochemical damage of the main wood compounds (lignin, cellulose, and hemicellulose) occurs by sunlight, especially UV radiation. Lignin decomposes by the UV radiation, causing the color change of archaeological wood surface (Jankowska, 2015). This process is slow and its impact is just on the thin layer of the wood surface (Sandberg, 1999).

2. Materials and Methods

The samples used for this research had been taken from the outdoor pine wood lintels in the mausoleum of Fatma Khatun (1283-1284) (AH 682-683). The wooden lintels were exposed to the influence of weathering factors which are varying in their amounts. Some of these lintels were exposed to the effect of weathering factors in the following sequence according to its amounts: (Moisture of "groundwater and relative humidity", sunlight, and temperature), this means that the moisture is the most influential weathering agent.

On the other hand, some of the other wooden lintels were exposed to the ef-

fect of weathering factors in the following sequence according to its amounts: (sunlight, temperature, and relative humidity), which means that the high temperature is the most influential weathering agent. To clarify the effect of the varying in weathering factors amounts on these wooden lintels; some of the analysis methods were used, such as:

1) Digital Microscope (DM): it was used to identify the wood types by examining the Transverse Section (TS) of the wooden lintels samples prepared for that purpose.

2) Scanning Electron Microscope (SEM): it was used to clarify the surface and anatomical changes of deteriorated wood. These samples were examined by SEM (JEOL 5500 LV, South Valley University, Qena, Egypt).

3) Fourier Transform Infrared Spectra (FTIR): it was used to clarify the changes in the main chemical compounds of the archaeological pine wood (the surface layer) resulting from the effects of weathering, comparing with a control sample (Unweathered). The FTIR was used in the spectral range 400 cm^{-1} to 4000 cm^{-1} by using (FTIR Jasco. 4100, South Valley University, Qena, Egypt).

3. Results and Discussion

3.1. Wood Identification

By using the digital microscope, the examination of the wooden lintels of Fatma Khatun mausoleum, in the transverse section (TS), showed the anatomical characteristic features of the pine wood "*Pinus sp.*". It can be observed the growth rings, earlywood tracheid (with the thin-walled), latewood tracheid (with the thick-walled), the rays, and resin canals (**Figure 3(B)** & **Figure 4(B)**, **Figure 5(B)** & **Figure 5(D)**). Through the examination, it was identified another kind of wood (Hardwood) wasn't broached in this research. It was used in one of the window lintels in the entry corridor of this mausoleum.

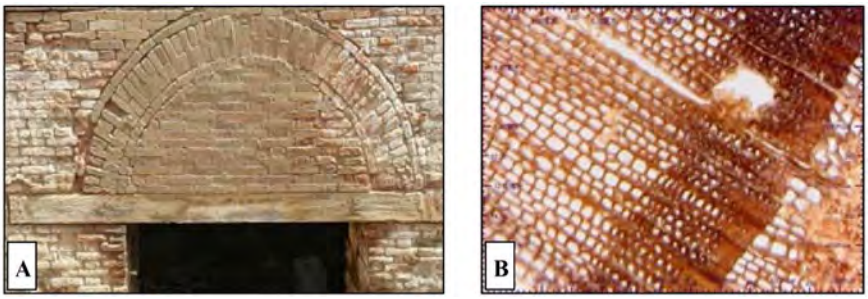

Figure 3. (A). The lintel of main door in the mausoleum dome chamber, (B). A cross-section of the pine wood (digital microscope).

3.2. Surface and Anatomical Changes

The pine wood (*Pinus sp.*) was used in the mausoleum of Fatma Khatun to make the lintels of the main door of the mausoleum dome chamber (**Figure 3(A)**), also it was used to make the window lintels in the outer portico and in the entry corridor of this mausoleum (**Figure 4(A)**, **Figure 5(A)** & **Figure 5(C)**).

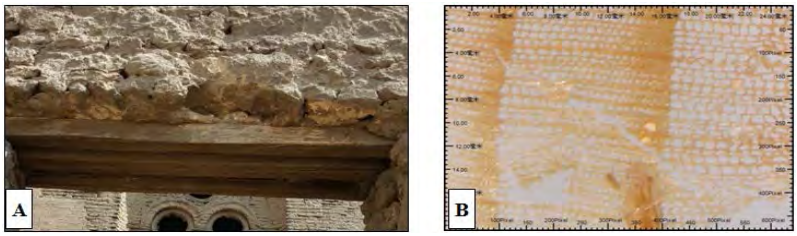

Figure 4. (A). The windows lintels in the outer portico and in the entry corridor of Fatma Khatun mausoleum, (B). A cross-section of the pine wood (digital microscope).

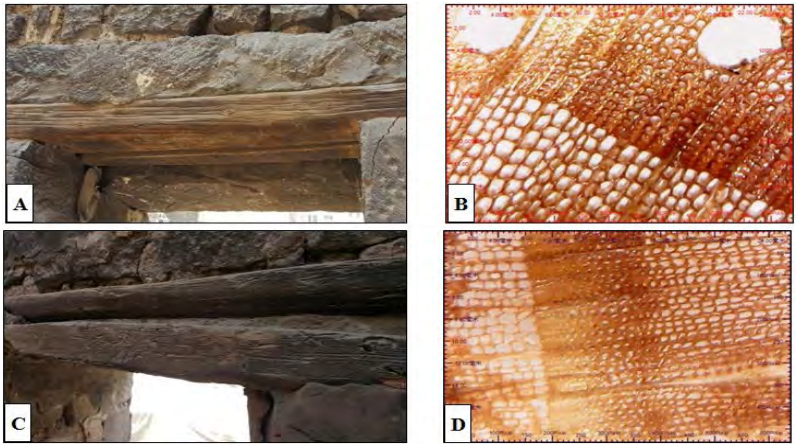

Figure 5. ((A) & (C)). The windows lintels in the outer portico and in the entry corri-dor of FatmaKhatun mausoleum, ((B) & (D)). A cross-section of the pine wood (digi-talmi-croscope).

The lintels of the door and of the windows are exposed directly to the effect of weathering factors surrounding these lintels (Moisture, temperature, and sunlight), but in varying quantities. For example, the lintels of the windows in the outer portico and in the entry corridor are located on high ground. Therefore, the lintels of the windows in this area are exposed to the effect of weathering factors in the following sequence: (sunlight, temperature, and relative humidity), and that according to the weathering factors the more concentrated. This arrangement was reflected in the appearance of these lintels.

The pine wood used in these lintels is very dry and that led to the spread of large longitudinal cracks in the same direction of the wood fibers. These cracks extend to the edge of these lintels (**Figure 6(C)** & **Figure 7(B)**). On the other side, we can observe the spread of fine cracks in the cell wall layers and also that there are many separations along the longitudinal axis of the wood cells (**Figure 8**). There are also some splits and fibers breaks on the surface and an erosion of the lintel's edges. The cracks appear on the wood surface as a result of repeated exposure to the wetness by the sources of moisture and to the drying by the high temperatures and air (Henriques & Azevedo, 2018).

The wood surface, directly exposed to weathering, appears uneven due to the difference in erosion rates between earlywood and latewood, and also between the knots and wood tissue (**Figure 7(A)** & **Figure 7(B)**). We can observe also

Figure 6. Spread of the different cracks on the pine wood surface, ((A), (B)) the lintel of the door in the mausoleum dome chamber, (C) the window lintel in the outer portico.

Figure 7. ((A), (B)) The window lintels in the outer portico showing the roughness of weathered wood surface, (C) the accumulated dust particles between the wood fibers, SEM micrograph. 50 μm.

Figure 8. SEM micrographs of the window lintels in the outer portico. (A) a longitudinal section showing the fragile and detached wood fibers, (B) a radial section showing the longitudinal cracks and the degradation of bordered pits (C) A cross-section showing the cracks and the separation of cell walls layers. (bar: (A) 200 μm, (b) 50 μm, (c) 10 μm).

that there are color changes spread irregularly on the surface of wood such as the presence of light brown areas and other areas with a dark brown color. The archaeological wood takes this dark color when it's not exposed directly to the effect of rain (Sandberg, 1999). The dust particles are widespread in the surrounding area of this mausoleum and for this reason, the dust particles accumulated and stuck on the wood surface as a result of wetness and drying exchanges (Ali, 2019) (**Figure 7(C)**).

The lintel of the main door in the mausoleum dome chamber was exposed to the effect of weathering factors in the following sequence: (Moisture of "groundwater and relative humidity", sunlight, and temperature). This arrangement was reflected in the appearance of the wood surface. The exposure of this lintel to high moisture levels, to direct sunlight and to high temperatures, especially in summer, led to the continuous exchange of wetness and dryness processes. These continuous processes were reflected in the appearance of the wood surface which appears fragile, spongy, and with incoherent fibers resulting from the breakdown of the wood components (Sandberg, 1999) (**Figure 9(C)** & **Figure 10**).

Figure 9. The lintel of the door in the mausoleum dome chamber (A) The roughness of weathered wood surface, (B) the wood knots affected by weathering, (C) the spongy appearance of the wood surface and the erosion of lintel edges.

Figure 10. SEM micrographs of the door lintel in the mausoleum dome chamber, (A) a longitudinal section showing the fragile and detached wood fibers, (B,C) a longitudinal section showing the detached wood tracheids. (bar: (A) 200 µm, (b) 500 µm, (C) 50 µm).

Various cracks are spread on the surface of this lintel but, the cracks which are perpendicular on the wood fibers direction are the most visible on the surface. These cracks exist just on the surface and don't penetrate to the mass of wood (**Figure 6(A)** & **Figure 6(B)**). The cracks come as a result of the repeated swelling and shrinking processes of the surface fibers. Comparing the number and size of the spread cracks on the windows lintels with other cracks on the door lintels, it can be seen that they're macro-cracks and more numerous in the window lintels. According to previous research (Sandberg, 1999), the direction of wood surface exposed to weathering has a significant part in the determination of the number and the size of cracks on the surface. For example, the number of cracks in the radial wood surface is less than the tangential wood surface. The presence of these different cracks on the archaeological wood surface lead to the penetration of weathering factors to the interior parts of the wood which get more damaged (Ali, 2019).

One of the more visible effects of weathering on this lintel is the variation of erosion rates between earlywood and latewood. The earlywood appears as carved lines on the wood surface extending along this lintel, with variable depth (1 - 2 mm). This erosion rate depends on the density of wood, therefore the low-density earlywood was the most affected by the weathering Factors (Unger et al., 2001; Williams, 2005) (**Figure 9(A)**). On the other side, It is also observed that the knots of wood were affected by weathering factors, as there was significant erosion, some cracks, and a loss of some of its apart (**Figure 9(B)**).

There are various color changes spread over the surface of this lintel. The lin-

tel parts adjacents to walls tend to the white or gray, while the other parts tend to the brown. This gray layer was resulted from the exposure of this lintel to the high levels of moisture and the direct exposure to sunlight, also it may be caused by the effect of the fungus (Yildiz et al., 2018). A large amount of dirt particles accumulates on the surface of this lintel, which is one of the important agents of the archaeological wood surface deterioration (William, 1983) (**Figure 11**).

A remarkable erosion was noticed in the lintel edges, especially the parts adjacents to the wall. This loss in these parts can be explained as follows: the wooden lintels are in direct contact with the walls and absorb water mixed with salts and other large quantities of soluble building materials. Because of high temperature, these materials crystallize on the surface, and between the fibers and with the effect of wind, these materials fall out with some parts of the fragile wood from the surface (**Figure 9(C)**).

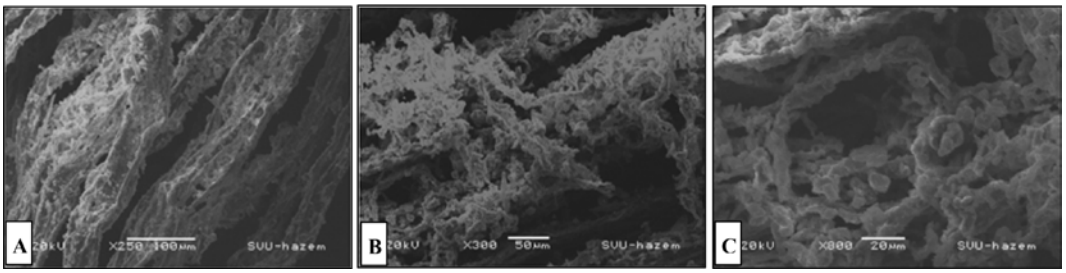

Figure 11. SEM micrographs of the door lintel in the mausoleum dome chamber, showing the detached wood fibers surrounded by dust particles. (A)-(C) longitudinal sections (bar: (A) 100μm, (B) 50 μm, (C) 20 μm).

3.3. FTIR Analysis

The FTIR spectra results of the pine wood samples (S1.control sample, S2 sample from the window lintel, and S3 sample from the door lintel) shown in the (**Table 1**) and (**Figure 12**). The FTIR spectra (region range between 400 - 4000 cm^{-1}) were used for the clarification of the differences between archaeological pine wood samples (weathered surface) and the control sample (unweathered sample).

By the comparison of the FTIR spectra between the archaeological pine wood samples (that were taken from the deteriorated wood surface) and the control samples (unweathered), we can understand the extent of chemical changes in the surface of this archaeological wood. This research shows a lot of changes in the bands of cellulose, hemicellulose, and lignin between the degraded wood and the control samples. It can be clarified as follows: The O-H band stretching around (3400 - 3420 cm^{-1}) shifted from 3419 cm^{-1} at sample S1 (the control sample) to a lower wavenumber at 3409 cm^{-1} for sample S2 and at 3408 cm^{-1} for sample S3. The absorption increased in the samples S3 and S2 as a result of the increase in the degradation of these samples (El Hadidi, 2017) and the hydroxyl groups oxidation (El-Hadidi & Darwish, 2008). The wide band around 3420 cm^{-1} in the archaeological wood samples were divided into two peaks (bands): for sample S2, the two peaks appear at 3409 cm^{-1} and 3527 cm^{-1}, for sample S3 the two

Table 1. FTIR Bands of the control sample (S1), the window lintel in the outer portico (S2 sample), and the door lintel in the mausoleum dome chamber (S3 sample).

Band position (cm^{-1})	Bands assigned *and Functional group*	References of the FT-IR bands	Wavenumber (cm^{-1})/absorptions		
			Sample S1	Sample S2	Sample S3
3200 - 3460 cm^{-1}	O-H stretching in carbohydrate and lignin	(Popescu et al., 2011a)	3419/62.41	3409/63.15 3527/67.42	3408/60.15 3527/65.54
2842 - 2935 cm^{-1}	C-H stretching (methyl and methylene groups)	(Pandey, 1999)	2937/85.34	2895/94.38	2938/90.97
1731 - 1739 cm^{-1}	C=O stretching (unconjugated ketones) in hemicellulose	(Shi et al., 2012; Yilgor et al., 2013; Özgenç et al., 2018)	1727/84.02	-	1732/87.46
1640 cm^{-1}	Absorbed water	(El Hadidi & Darwish, 2014)	1645/79.18	1637/74.41 1625/74.51	1647/73.54 1636/72.89 1624/72.43
1595 cm^{-1}	Aromatic skeletal, C=O stretch in lignin	(Han et al., 2020)	1592/84.11	1595/86.84	1594/87.92
1506 - 1515 cm^{-1}	C=C stretching, Aromatic ring (lignin)	(Bodîrlău & Teacă, 2009; Gonultas & Candan, 2018)	1511/78.06	1508/89.24	1507/89.56
1460 cm^{-1}	C-H asymmetric deformations in $-CH_3$ and $-CH_2-$	(Jahan & Mun, 2006; Huang et al., 2012)	1461/78.27	1461/82.35	-
1425 cm^{-1}	CH_2 bending cellulose	(El Hadidi, 2017)	1426/77.13	1420/83.32	1418/78.53
1375 cm^{-1}	CH bending in cellulose	(Poletto et al., 2012; Lionetto et al., 2012; El Hadidi, 2017)	1373/76.37	1384/79.7	1384/53.62
1335 cm^{-1}	OH (plane bending in cellulose 'amorphous')	(Colom et al., 2003; Lionetto et al., 2012; El Hadidi, 2017)	-	-	1336/78.67
1316 cm^{-1}	CH_2 wagging (crystalline cellulose)	(Colom et al., 2003; Lionetto et al., 2012; El Hadidi, 2017)	1318/76.94	1320/79.76	1320/79.90
1269 cm^{-1}	guaiacyl ring, C-O in lignin	(Pandey, 1999; Popescu et al., 2006)	1269/72.91	1269/81.77	-
1235 cm^{-1}	Acetyl and carboxyl vibrations and C=O stretching in Xylan and lignin	(Yilgor et al., 2013)	1233/74.14	-	-
1159 cm^{-1}	C–O–C asymmetric stretching vibrations (Carbohydrate)	(Andriulo et al., 2016; Traoré et al., 2018)	1159/69.09	-	-
897 cm^{-1}	C-H deformation in cellulose	(Zhou et al., 2018)	896/80.09	895/85.46	863/89.65
806 cm^{-1}	Aromatic C-H (out of planedeformations) in lignin	(Evans, 1991; Xing et al., 2015; Traoré et al., 2018)	806/81.23	807/84.77	808/87.07

peaks appear at 3408 cm^{-1} and 3527 cm^{-1}. The band at 3527 cm^{-1} is related to the absorbed water bound and the intramolecular H-bond in lignin (Popescu et al., 2011b). According to a previous literature, this stretching mode of H_2O molecules is caused by the high level of moisture surrounding these wood lintels (El-Hadidi & Darwish, 2008).

The FTIR spectra of sample S2 shows a decrease in the absorbance at 2895 cm^{-1} and 2939 cm^{-1} (C-H stretching) bands, for sample S3 the band around 2890 cm^{-1} is disappeared and there is a decrease in absorbance at 2895 cm^{-1}. This decrease comes as a result of the degradation of cellulose and the changes in its

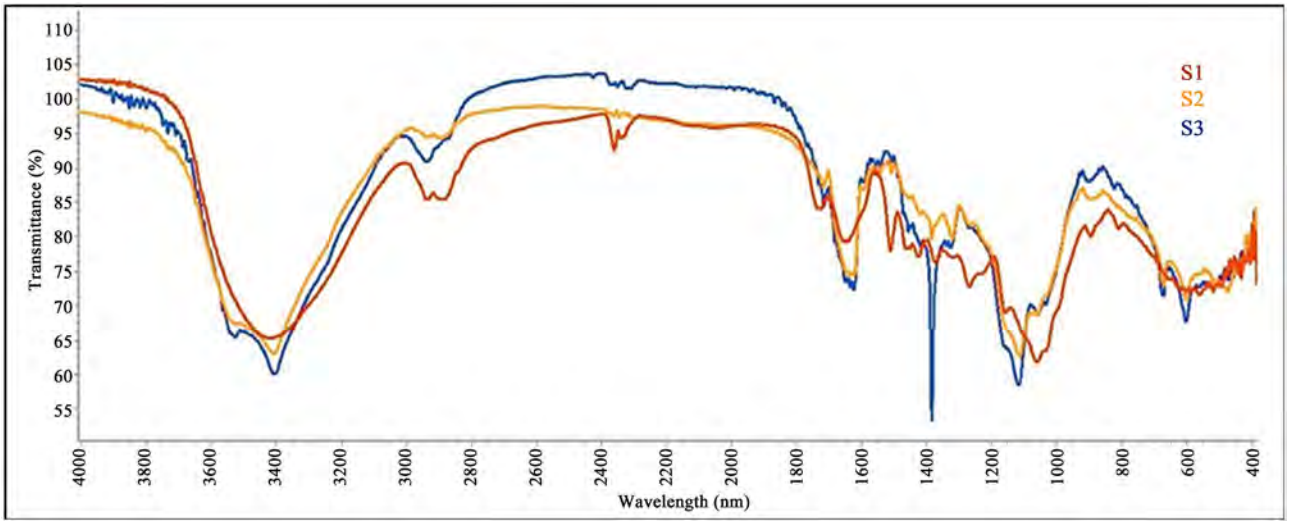

Figure 12. FTIR spectra of the control sample (S1), the window lintel in the outer portico (S2 sample), and the door lintel in the mausoleum dome chamber (S3 sample).

crystallinity level (Kubovský et al., 2020).

At the band around 1640 cm^{-1} (C=O stretching), which refers to H_2O absorption, there is a remarkable increase in band intensity. This corresponds to the increase and the split in the O-H stretching band around 3420 - 3527 cm^{-1}. This band comes as a result of the water absorption from the surrounding environment. The obvious multiplication of carbonyl bands in this zone is resulting from the degradation of lignin and cellulose (El-Hadidi & Darwish, 2008).

The band at 1739 cm^{-1} (C=O stretch in un-conjugated ketones) concerns hemicellulose. This band disappeared in the sample S2, while the absorption intensity at sample S3 decreased obviously. The decrease in this band is caused by the deterioration of the acetyl group and hemicellulose by the effect of weathering factors (Reinprecht et al., 2018; Yildiz et al., 2018; Iruela, 2020).

The bands which concern lignin were found at 1595 cm^{-1}, 1511 cm^{-1} and 1269 cm^{-1}. In addition to that, the band at 1460 cm^{-1} concern lignin and carbohydrates (Pandey & Pitman, 2003). All bands of lignin registered a significant decrease in absorbance. The absorption band around 1595 cm^{-1} (aromatic skeletal) appears in sample S1 as a shoulder. As for the archaeological samples, a decrease in absorption intensity was observed around the band 1595 cm^{-1} which appeared very weak in samples S2 and S3. According to some previous researches, the changes and the absorption decrease at this band and that may be due to the presence of water in these samples (Fors & Richards, 2010), and also to the effect of the methoxy (O-CH) groups of the guaiacyl rings (Zhang et al., 2009).

The band around 1505 - 1511 cm^{-1} (aromatic skeletal) is used to assess the content of Lignin in wood samples. Comparing samples S2 and S3 with the S1 sample, there is a shift of this band and a remarkable decrease in intensity of the bands at 1508 cm^{-1} for S2 and at 1507 cm^{-1} for S3 which appear as very weak peaks. This decrease indicates the effect of weathering factors on the aromatic rings (Zhang et al., 2009). Previous research reported that this decrease is re-

sulting from the methoxyl groups decrease and from the loss of syringyl units of lignin (Kubovský et al., 2020). Weathering caused a decrease in the intensity of the 1269 cm^{-1} band (guaiacyl ring breathing with C-O stretching) (Lionetto et al., 2012) in the archaeological samples. It was a very clear band in the control sample, but it appeared as a shoulder in the sample S2, and disappeared in the sample S3. The band at 1460 cm^{-1} (asymmetric CH deformations in lignin) (Kubovský et al., 2020) in sample S2 was observed very weak, while it was absent in sample S3.

The absorption bands around 1373 cm^{-1}, 1336 cm^{-1}, 1317 cm^{-1}, 1159 cm^{-1} and 897 cm^{-1} refer to cellulose. The cellulose band at 1373 cm^{-1} appeared in the control sample, while it appeared in the archaeological samples at 1384 cm^{-1}. This band in sample S2 decreased in absorbance and appeared as a weak band. In sample S3, the band at 1384 cm^{-1} increased in absorbance and appeared as a very strong band. The increase in intensity in this band refers to the depolymerization of cellulose which is intimately related to the decrease or the disappearance of the lignin band around 1510 cm^{-1} (Genestar & Palou, 2006).

There was a decrease in the band intensity that was noted in the band at1425 cm^{-1} (CH_2 bending cellulose, "crystallized I and amorphous cellulose") (El Hadidi, 2017). This band shifted also to lower wavelengths in the archaeological samples: it became at 1420 cm^{-1} in sample S2 and at 1418 cm^{-1} in sample S3, and that indicates the extent of the cellulose damage resulting from the weathering factors

The bands at 1335 cm^{-1} and at 1316 cm^{-1} refer to the wood cellulose, in the control sample (S1) these bands were observed as weak bands with a shoulder at 1318 cm^{-1}. In the archaeological samples (S2, S3), these bands decreased in absorption compared with the S1 sample. However, these bands can be observed as two bands in sample S3 around 1320 cm^{-1} and 1336 cm^{-1}, while in sample S2, only one band appeared as one peak at 1320 cm^{-1}. Previous research stated that the decrease of absorption and the two similar bands in this area were a result of the increase of the content of the crystallized cellulose (Colom et al., 2003). The band at 1235 cm^{-1} (C=O in xylan-lignine), disappeared in samples S2 and S3 and that comes as a result of the degradation of xylan and the lignin changes (Shi et al., 2012). The peak at 1159 cm^{-1} (C–O–C asymmetric stretching vibrations in cellulose and hemicellulose) disappeared in samples S2 and S3. This means that there is a big loss in the degree of cellulose polymerization (breaking the chains of cellulose) (Darwish et al., 2013; Hamed et al., 2020).

The peak at 897 cm^{-1} (C–H deformation of cellulose) (Reinprecht et al., 2018) decreased significantly in intensity. It seems like a very weak peak in the archaeological samples (S2 and S3). This decrease indicates the decrease of the amorphous cellulose (Kubovský et al., 2020). The peaks at 806 cm^{-1} (the ring of benzene) decreased substantially in intensity and appeared as a very weak peak. There was a similar result in previous research which reported that the delignification from the softwood was the reason for these changes (Xing et al., 2015).

The results and findings summary: it's so clear that the pine wood which was exposed in its surface to weathering factors with high levels of moisture, was damaged more than the pine wood that was exposed to normal levels of relative humidity. We find that the outer surface of the wood exposed to high levels of moisture became very brittle, pale, swollen, and its fibers lack bonding especially in the areas nearby the walls.

The FTIR spectra showed that the main chemical components of the two archaeological wood samples were remarkably affected by the weathering Factors. In these samples, it was observed a decrease in most of the cellulose, hemicellulose, and lignin bands. There are some other bands that have disappeared such as the bands at 1235 cm^{-1} and at 1159 cm^{-1} for the two samples (S1 and S2). For the bands around 1269 cm^{-1}, 1460 cm^{-1}, and 2890 cm^{-1}, they disappeared in sample S3. Also, the band around 1739 cm^{-1} disappeared in sample S2. The FTIR analysis results indicate that the door lintel, surrounded by high levels of moisture in the mausoleum dome chamber, is the most affected by the weathering factors. It appears that the decrease in most of the cellulose, hemicellulose, and lignin bands was more than in the window lintels of the outer portico which are surrounded by low levels of humidity. There is a remarkable increase at the 1384 cm^{-1} band which is resulted from the depolymerization of cellulose (Genestar & Palou, 2006). It is observed also that the bands of lignin at 1460 cm^{-1}, 1268 cm^{-1}, and 1235 cm^{-1} disappeared and this explains the obvious detachment between the wood surface fibers.

4. Conclusion

In general, the evaluation results of the archaeological wood deterioration are very important to identify the deterioration patterns and the changing of environmental conditions surrounding this archaeological wood. Also, this evaluation enables us to use the appropriate methods and materials of treatment that must be selected according to the status of the wooden artifacts (El Hadidi, 2017).

In the archaeological and historical buildings, all the outdoor wooden artifacts are exposed to the influence of the surrounding weathering factors. It is remarkable in this research that all of the outdoor lintels in the mausoleum of Fatma Khatun are exposed to the directly weathering agents, but with a disparity in its amounts. Some of these lintels (the lintels of the main door in the mausoleum dome chamber) were exposed to the effect of weathering factors in the following sequence according to its amounts: (Moisture of "groundwater and relative humidity", sunlight, and temperature). Some of other lintels (the window lintels in the outer portico and in the entry corridor of this mausoleum) were exposed to the effect of weathering factors in the following sequence according to its amounts: (sunlight, temperature, and relative humidity).

The analysis was made by using the Digital Microscope (DM), Scanning Electron Microscope (SEM), and Fourier Transform Infrared Spectra (FTIR), which

showed that the disparity in the amounts of the weathering agents had a clear effect on the wood appearance, the wood cells, and on its main chemical components.

The wooden lintels that exposed to the weathering factors with high levels of moisture were damaged more than the wooden lintels that were exposed to high temperature and normal levels of relative humidity. We find that the surface of the wood exposed to high levels of moisture appears very brittle, pale, swollen, and its surface fibers lack bonding, especially in the areas nearby the walls. Also, the FTIR analysis results indicate that the wooden lintel which was surrounded by high levels of moisture, is the most affected by the weathering factors. The sample of this lintel showed a decrease in most of the cellulose, hemicellulose, and lignin bands. The disappearance of some lignin bands at 1460 cm^{-1}, 1268 cm^{-1}, and at 1235 cm^{-1} explains the obvious detachment between the wood surface fibers. This research contributes to change the researchers' perspective when they study the effect of weathering factors on archaeological wood because this research recommends to arrange these factors according to its amounts. In this study, we found that the arrangement of weathering agents according to their amounts was clearly reflected on the external appearance and the on main chemical compounds of archaeological pine wood.

Conflicts of Interest

The author declares no conflicts of interest regarding the publication of this paper.

References

Ali, M. (2019). *The Deterioration of Domestic Wooden Surfaces of Historical Buildings in Upper Egypt* (pp. 3-24). Athens: ATINER'S Conference Paper Series, No. ART2019-2697.

Andriulo, F. et al. (2016). Nanotechnologies for the Restoration of Alum-Treated Archaeological Wood. *Applied Physics A, 122,* 322. https://doi.org/10.1007/s00339-016-9833-0

Bodîrlău, R., & Teacă, C. A. (2009). Fourier Transform Infrared Spectroscopy and Thermal Analysis of Lignocellulose Fillers Treated with Organic Anhydrides. *Romanian Journal of Physics, 54,* 93-104.

Colom, X. et al. (2003). Structural Analysis of Photodegraded Wood by Means of FTIR Spectroscopy. *Polymer Degradation and Stability, 80,* 543-549. https://doi.org/10.1016/S0141-3910(03)00051-X

Darwish, S. et al. (2013). The Effect of Fungal Decay on Ficus Sycomorus Wood. *International Journal of Conservation Science, 4,* 271-282.

El Hadidi, N. (2017). Decay of Softwood in Archaeological Wooden Artifacts. *Studies in Conservation, 62,* 83-95. https://doi.org/10.1179/2047058415Y.0000000028

El Hadidi, N., & Darwish, S. (2014). Preliminary Study on the Different Effects of Consolidation Treatments in Heartwood and Sapwood of a Decayed Gymnosperm Wood. *Egyptian Journal of Archaeological and Restoration Studies, 4,* 1-11. https://doi.org/10.21608/ejars.2018.7269

El-Hadidi, N., & Darwish, S. (2008). The Use of Acids and Alkalis in Cleaning Archaeological Wood. *International Conference on Giza through the Ages, Faculty of Archaeology,* Cairo, 4-6 March 2008.

Evans, P. A. (1991). Differentiating "Hard" from "Soft" Woods Using Fourier Transform Infrared and Fourier Transform Raman Spectroscopy. *Spectrochim Acta A, 47,* 1441-1447. https://doi.org/10.1016/0584-8539(91)80235-B

Feist, W. C. (1983). Weathering and Protection of Wood. *Proceedings, Seventy-Ninth Annual Meeting of the American Wood-Preservers' Association,* Vol. 79, 195-205.

Feist, W. C. (1990). Outdoor Wood Weathering and Protection. In *Archaeological Wood: Properties, Chemistry and Preservation* (pp. 263-298). Washington DC: American Chemical Society. https://doi.org/10.1021/ba-1990-0225.ch011

Fors, Y., & Richards, V. (2010). The Effects of the Ammonia Neutralizing Treatment on Marine Archaeological Vasa Wood. *Studies in Conservation, 55,* 41-54. https://doi.org/10.1179/sic.2010.55.1.41

Genestar, C., & Palou, J. (2006). SEM-FTIR Spectroscopic Evaluation of Deterioration in an Historic Coffered Ceiling. *Analytical and Bioanalytical Chemistry, 384,* 987-993. https://doi.org/10.1007/s00216-005-0243-y

Gonultas, O., & Candan, Z. (2018). Chemical Characterization and FTIR Spectroscopy of Thermally Compressed Eucalyptus Wood Panels. *Maderas: Ciencia y Tecnologia, 20,* 431-442. https://doi.org/10.4067/S0718-221X2018005031301

Hamed, S. A. M. (2014). Investigation of Deterioration in Archaeological Wood Used in Architectural Elements: Microscopic Study. In A. Méndez-Vilas (Ed.), *Microscopy: Advances in Scientific Research and Education* (Vol. 2, pp. 857-862). Badajoz: Formatex Research Center.

Hamed, S. A. M. et al. (2020). Investigating the Impact of Weathering and In-door Aging on Wood Acidity Using Spectroscopic Analyses. *BioResources, 15,* 6506-6525.

Han, L. et al. (2020). Even Visually Intact Cell Walls in Waterlogged Archaeological Wood Are Chemically Deteriorated and Mechanically Fragile: A Case of a 170 Year-Old Shipwreck. *Molecules, 25,* 1113. https://doi.org/10.3390/molecules25051113

Henriques, D. F., & Azevedo, A. C. B. (2018). Outdoor Wood Weathering and Protection. *Construction Pathology, Rehabilitation Technology and Heritage Management,* Caceres, 15-18 May 2018, 2007-2015.

Huang, Y. et al. (2012). Analysis of Lignin Aromatic Structure in Wood Based on the IR Spectrum. *Journal of Wood Chemistry and Technology, 32,* 294-303. https://doi.org/10.1080/02773813.2012.666316

Iruela, A. G. (2020). Effect of Degradation on Wood Hygroscopicity: The Case of a 400-Year-Old Coffin. *Forests, 11,* 712. https://doi.org/10.3390/f11070712

Jahan, M. S., & Mun, S. P. (2006). Characteristics of Milled Wood Lignins Isolated from Different Ages of Nalita Wood (*Trema orientalis*). *Cellulose Chemistry and Technology, 40,* 457-467.

Jankowska, A. (2015). The Study of Influence Artificial Weathering on Color Changes of Selected Wood Species from Africa. *Forestry and Wood Technology, 92,* 131-136.

Kubovský, I. et al. (2020). Structural Changes of Oak Wood Main Components Caused by Thermal Modification. *Polymers, 12,* 485. https://doi.org/10.3390/polym12020485

Lionetto, F. et al. (2012). Monitoring Wood Degradation during Weathering by Cellulose Crystallinity. *Materials, 5,* 1910-1922. https://doi.org/10.3390/ma5101910

Oberhofnerová, E. et al. (2017). The Effect of Natural Weathering on Untreated Wood Surface. *Maderas. Ciencia y Tecnología, 19,* 173-184.

Özgenç, Ö. et al. (2018). ATR-FTIR Spectroscopic Analysis of Thermally Modified Wood Degraded by Rot Fungi. *Drewno, 61,* 91-105.

Pandey, K. K. (1999). A Study of Chemical Structure of Soft and Hardwood and Wood Polymers by FTIR Spectroscopy. *Journal of Applied Polymer Science, 71,* 1969-1975. https://doi.org/10.1002/(SICI)1097-4628(19990321)71:12<1969::AID-APP6>3.0.CO;2-D

Pandey, K. K., & Pitman, A. J. (2003). FTIR Studies of the Changes in Wood Chemistry Following Decay by Brown-Rot and White-Rot Fungi. *International Biodeterioration & Biodegradation, 52,* 151-160. https://doi.org/10.1016/S0964-8305(03)00052-0

Poletto, M. et al. (2012). Structural Differences between Wood Species: Evidence from Chemical Composition, FTIR Spectroscopy, and Thermogravimetric Analysis. *Journal of Applied Polymer Science, 126,* E336-E343. https://doi.org/10.1002/app.36991

Popescu, C. et al. (2011a). Structural Analysis of Photodegraded Lime Wood by Means of FT-IR and 2D IR Correlation Spectroscopy. *International Journal of Biological Macromolecules, 48,* 667-675. https://doi.org/10.1016/j.ijbiomac.2011.02.009

Popescu, C. M. et al. (2006). Analytical Methods for Lignin Characterization. II. Spectroscopic Studies. *Cellulose Chemistry and Technology, 40,* 597-621.

Popescu, M. et al. (2011b). Evaluation of Morphological and Chemical Aspects of Different Wood Species by Spectroscopy and Thermal Methods. *Journal of Molecular Structure, 988,* 65-72. https://doi.org/10.1016/j.molstruc.2010.12.004

Reinprecht, L. et al. (2018). The Impact of Natural and Artificial Weathering on the Visual, Colour and Structural Changes of Seven Tropical Woods. *European Journal of Wood and Wood Products, 76,* 175-190. https://doi.org/10.1007/s00107-017-1228-1

Sandberg, D. (1999). Weathering of Radial and Tangential Wood Surfaces of Pine and Spruce. *Holzforschung, 53,* 355-364. https://doi.org/10.1515/HF.1999.059

Shi, J. et al. (2012). FTIR Studies of the Changes in Wood Chemistry from Wood Forming Tissue under Inclined Treatment. *Energy Procedia, 16,* 758-762. https://doi.org/10.1016/j.egypro.2012.01.122

Teles, C. D. M., & Valle, Â. (2001). Wood Structures: Acting before Deterioration. In P. B. Lourenço, & P. Roca (Eds.), *Historical Constructions* (pp. 857-866). Guimarães: University of Minho.

Traoré, M. et al. (2018). Differentiation between Pine Woods According to Species and Growing Location Using FTIR-ATR. *Wood Science and Technology, 52,* 487-504. https://doi.org/10.1007/s00226-017-0967-9

Unger, A. et al. (2001). *Conservation of Wood Artifacts* (p. 48). Heidelberg: Springer-Verlagberin.

Wiemann, M. C. (2010). Characteristics and Availability of Commercially Important Woods. In *Wood Handbook—Wood as an Engineering Material, Centennial Edition* (p. 1). Madison, WI: Forest Products Laboratory.

William, C. F. (1983). Weathering and Protection of Wood. *Proceedings, Seventy-Ninth Annual Meeting of the American Wood-Preservers' Association,* Kansas City, 17-20 April, 195-205.

Williams, R. S. (2005). Weathering of Wood. In *Handbook of Wood Chemistry and Wood Composites* (p. 167). Boca Raton, FL: CRC Press.

Xing, D. et al. (2015). Effect of Artificial Weathering on the Properties of Industrial-Scale Thermally Modified Wood. *BioResources, 10,* 8238-8252. https://doi.org/10.15376/biores.10.4.8238-8252

Yildiz, S. et al. (2018). The Effects of Natural Weathering on the Properties of Heat-

Treated Alder Wood. *BioResources, 6,* 2504-2521.

Yilgor, N. et al. (2013). Evaluation of Fungal Deterioration in *Liquidambar orientalis* Mill. Heartwood by FT-IR and Light Microscopy. *BioResources, 8,* 2805-2826. https://doi.org/10.15376/biores.8.2.2805-2826

Zhang, J. et al. (2009). Weathering of Copper-Amine Treated Wood. *Applied Surface Science, 256,* 842-846. https://doi.org/10.1016/j.apsusc.2009.08.071

Zhou, Y. et al. (2018). Degradation Features of Archaeological Wood Surface to Deep Inside a Case Study on Wooden Boards of Marquis of Haihun's Outer Coffin. *Wood Research, 63,* 419-430.

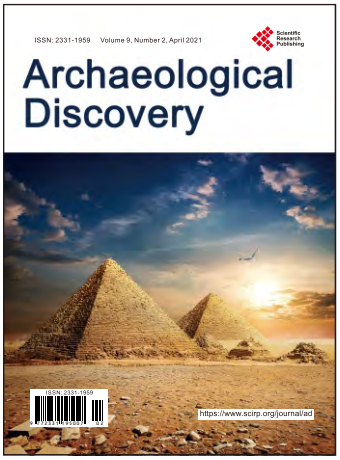

Call for Papers

Archaeological Discovery

ISSN Print: 2331-1959 **ISSN Online: 2331-1967**

https://www.scirp.org/journal/ad

Archaeological Discovery (AD) is an international journal dedicated to the latest advancement in the study of Archaeology. The goal of this journal is to provide a platform for scientists and academicians all over the world to promote, share, and discuss various new issues and developments in different areas of Archaeological studies.

Subject Coverage

All manuscripts must be prepared in English, and are subject to a rigorous and fair peer-review process. Accepted papers will immediately appear online followed by printed hard copy. The journal publishes original papers covering a wide range of fields but not limited to the following:

- Aerial Archaeology
- Archaeological Method and Theory
- Archaeological Science
- Archaeometry
- Art Archaeology
- Environmental Archaeology
- Ethnoarchaeology
- Experimental Archaeology
- Field Archaeology
- Geoarchaeology
- Historical Archaeology
- Island and Coastal Archaeology
- Lithic Studies
- Maritime Archaeology
- Prehistoric Archaeology
- Religious Archaeology
- Social Archaeology
- Underwater Archaeology
- World Archaeology
- Zooarchaeology

We are also interested in: 1) Short reports — 2-5 page papers in which an author can either present an idea with a theoretical background but has not yet completed the research needed for a complete paper, or preliminary data; 2) Book reviews — Comments and critiques, special peer-reviewed issue for colloquia, symposia, workshops.

Website and E-Mail

https://www.scirp.org/journal/ad **E-mail: ad@scirp.org**

What is SCIRP?

Scientific Research Publishing (SCIRP) is one of the largest Open Access journal publishers. It is currently publishing more than 200 open access, online, peer-reviewed journals covering a wide range of academic disciplines. SCIRP serves the worldwide academic communities and contributes to the progress and application of science with its publication.

What is Open Access?

All original research papers published by SCIRP are made freely and permanently accessible online immediately upon publication. To be able to provide open access journals, SCIRP defrays operation costs from authors and subscription charges only for its printed version. Open access publishing allows an immediate, worldwide, barrier-free, open access to the full text of research papers, which is in the best interests of the scientific community.

- High visibility for maximum global exposure with open access publishing model
- Rigorous peer review of research papers
- Prompt faster publication with less cost
- Guaranteed targeted, multidisciplinary audience

Scientific Research Publishing

Website: https://www.scirp.org

Subscription: sub@scirp.org

Advertisement: service@scirp.org